RSC Advances

PAPER

View Article Online
View Journal | View Issue

Cite this: *RSC Adv.*, 2019, **9**, 24117

Synthesis, structural studies and biological properties of some phosphono-perfluorophenylalanine derivatives formed by S_NAr reactions†‡

Joanna Kwiczak-Yiğitbaşı,[ab] Jean-Luc Pirat,[b] David Virieux,[b] Jean-Noël Volle,*[b] Agnieszka Janiak,[a] Marcin Hoffmann,[a] Jakub Mrzygłód,[a] Dariusz Wawrzyniak,[c] Jan Barciszewski[cd] and Donata Pluskota-Karwatka*[a]

Several novel phosphono-perfluorophenylalanine derivatives, as mimetics of phenylalanine, were synthesized by subjecting diethyl (2-(perfluorophenyl)-1-(phenylamino)ethyl)-phosphonate to S_NAr reactions with different types of nucleophiles such as thiols, amines and phenols. The structure of the products was confirmed using spectroscopic and spectrometric techniques. For two compounds X-ray single crystal diffraction analysis and DFT investigations were performed providing information in regard to the preferable conformation, hydrogen bonds and other interactions. The antiproliferative potency of some of the new phosphono-perfluorophenylalanine derivatives obtained as well as representatives of previously synthesized perfluorophenyl phosphonate analogues of phenylalanine was studied on selected glioma cell lines. Preliminary evaluation of the compounds drug likeness was examined with respect to Lipinski's and Veber's rules, and showed that they meet the criteria perfectly. MTT (3-(4,5-dimethyl-2-thiazolyl)-2,5-diphenyl-2*H*-tetrazolium bromide) assay results demonstrated that the compounds exhibit moderate activity against the glioblastoma multiforme cell lines (T98G and U-118 MG). Moreover most of the studied S_NAr reaction products displayed significantly higher inhibitory activity against both cancer cell lines than the parent diethyl (2-(perfluorophenyl)-1-(phenylamino)ethyl) phosphonate.

Received 26th May 2019
Accepted 16th July 2019

DOI: 10.1039/c9ra03982a

rsc.li/rsc-advances

1. Introduction

Chemistry of α-aminophosphonates has played a significant role in the development of organophosphorus compounds, and still remains a field of great interest.[1–3] As structural analogues of α-amino acids, α-aminophosphonates have found application in organic and medicinal chemistry,[4] mainly due to their anticancer,[5–9] antiviral[10] and antibacterial[11,12] activities. Moreover, phosphonates represent classical phosphate bioisosters, in which the labile O–P bond is replaced by an enzymatically and chemically stable C–P bond. This change makes α-aminophosphonates structurally similar to phosphate esters or anhydrides, yet increases their stability under physiological and chemical conditions.[13,14] Also, the tetrahedral geometry on the phosphorus atom mimics the transition state of peptide hydrolysis thus, α-aminophosphonates can act as enzyme inhibitors.[15–17]

Among α-aminophosphonates, the fluorinated ones constitute a particularly important group of compounds. The incorporation of fluorine atoms in the structure of α-aminophosphonates provides access to more lipophilic molecules, which often exhibit better biological activities than the parent compounds.[18,19] What is more, the presence of fluorine and phosphorus atoms in the α-aminophosphonates structure gives us a chance to use ^{19}F and ^{31}P NMR spectroscopy to follow the location and to study the molecular interactions in biological systems.[20,21]

Introduction of fluorine has also become an important strategy in protein biochemistry. Fluorinated amino acids serve as powerful tools for exploring polar π-interactions in proteins,[22,23] and enabling novel recognition mechanisms for protein design.[24–26] Heavily fluorinated aromatic residues are

[a]*Adam Mickiewicz University in Poznań, Faculty of Chemistry, Umultowska 89b, 61-614 Poznań, Poland. E-mail: donatap@amu.edu.pl*

[b]*AM2N, UMR 5253, ICGM, ENSCM, 8 Rue de L'Ecole Normale, 34296 Montpellier Cedex 5, France. E-mail: jean-noel.volle@enscm.fr*

[c]*Institute of Bioorganic Chemistry, Polish Academy of Sciences, Noskowskiego 12/14, 61-704 Poznań, Poland*

[d]*NanoBioMedical Center of Adam Mickiewicz University, Umultowska 85, 61-614, Poznań, Poland*

† Dedication to Professor Henryk Koroniak in honour of his 70th birthday.

‡ Electronic supplementary information (ESI) available. CCDC 1912530 and 1912531. For ESI and crystallographic data in CIF or other electronic format see DOI: 10.1039/c9ra03982a

particularly desirable because multifluorination gives maximum electronic perturbation of aromatic rings.

Fluorinated aromatic rings may undergo nucleophilic aromatic substitution reactions (S_NAr). Due to higher electronegativity of carbon comparing to hydrogen, benzene exhibits a negative potential on the π face and a positive one around the periphery.[27] Fluorine as strongly electronegative element, reverses this distribution to give a negative potential on the periphery and a positive on the aromatic ring,[27] or, as theoretical studies suggest, localized more to carbon skeleton than the π-electrons cloud.[28,29] Thus fluorination clearly enhances the rate of nucleophilic attack. In general, the reaction of pentafluorophenyl moiety is highly regioselective; nucleophile replaces almost exclusively the fluorine atom in the *para* position.[27] The S_NAr reactions found application for fluorinated amino acids syntheses. Regioselective nucleophilic addition–elimination reaction of pentafluorobenzyl moiety was the key step on the synthetic route to tetrafluorotyrosine.[30] This strategy was then extended to preparation of a series of *para*-substituted tetrafluorophenylalanines.[31] Also cysteine arylation was achieved *via* S_NAr reactions.[32] Reaction between cysteine thiolate and perfluoroaromatic molecules afforded exclusively 1,4-disubstituted products. Such approach enabled selective modification of cysteine residues in unprotected peptides.[32]

As part of our investigations, we have recently reported a convenient synthetic method for the preparation of a series of phosphonate analogues of phenylglycine, homophenylalanine, and phenylalanine that differ in the number and position of fluorine atoms in the phenyl ring.[33,34] These studies were supported by single-crystal X-ray diffraction analysis and quantum chemical calculations that provided information concerning the conformational preferences both in the solid and isolated states. Indeed, some of the obtained aminophosphonates underwent intramolecular S_NAr reactions yielding indolinylphosphonates as minor products.[33] Since S_NAr reaction is an attractive and effective way for modifying structure of fluorinated aromatic compounds, we decided to study the ability of the synthesized α-aminophosphonates to undergo such a transformation. It gave us a chance to obtain a library of diversely substituted α-aminophosphonates and opened a new perspectives to seek for original bioactive molecules. Therefore in this paper we describe the synthesis of *para* substituted derivatives of diethyl (2-(perfluorophenyl)-1-(phenylamino) ethyl)phosphonate **1a** (Scheme 1) as well as results of their X-ray and DFT studies. Structural variations on products were achieved by subjecting the phenylalanine analogue **1a** to reactions with various nucleophiles, *i.e.* thiols, amines and phenols (Scheme 1).

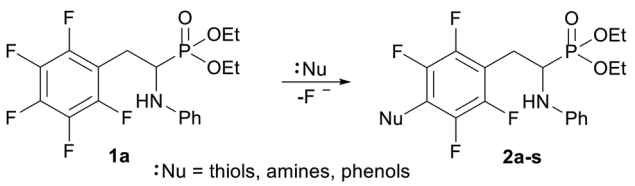

Scheme 1 Synthesis of **2a–s**.

Some of the phosphono-perfluorophenylalanine derivatives obtained together with representatives of previously synthesized[33] perfluorophenyl phosphonate analogues of phenylalanine were subjected to studies aimed at evaluation of the compounds antiproliferative potency on chosen glioblastoma multiforme (GBM) cell lines.

GBM is highly infiltrative tumour which displays extreme resistance to conventional radiotherapy and chemotherapy.[35] It contains self-renewing, tumorigenic cancer stem cells (CSCs) that contribute to tumour initiation and therapeutic resistance. These cells in malignant gliomas were called glioblastoma stem cells (GSCs).[36] Recent studies uncovered increased expression, aberrant localization and disturbed functions of certain cysteine cathepsins in GSCs.[37] Cathepsins B and L are overexpressed in glioma cells and responsible for glioblastoma cell invasion.[38,39] The scientific literature shows ability of aminophosphonic acids and aminophosphonates to act as inhibitors of esterases,[17,40] protease inhibitors[41] and cathepsins. Therefore, targeting cathepsin activity by specific protease inhibitors in GBM is a logical consequence and might interfere with proliferation, and migration to avoid recurrence of glioblastoma.

2. Results and discussion

2.1 Synthesis

Diethyl (2-(perfluorophenyl)-1-(phenylamino)ethyl)phosphonate (**1a**, Scheme 1) was subjected to S_NAr reactions with thiols, amines and phenols resulted in the formation of *para*-substituted products (**2a–s**, Scheme 1, Table 1) with full regioselectivity.

Several conditions already described in the literature for these S_NAr reactions[32,42–44] were applied to the reaction of **1a** with both hard and soft nucleophiles. Hard nucleophiles, such as hydroxide or alcoxides, had a clear tendency to attack the phosphonate ester while soft nucleophiles cleanly afforded the S_NAr reactions (Table 1).

Following the procedure developed by Spokoyny *et al.*,[32] thiols reacted smoothly in DMF, in the presence of tris(hydroxymethyl)aminomethane (TRIS) at room temperature within short reaction time (2 h). In order to study the scope of the reaction, syntheses with different thiols were performed (Table 1, entries 1–10). Nucleophilic aromatic substitution of **1** with thiophenols (Table 1, entries 1–7) occurred in good to excellent yields (76–95%). Both EDG (Table 1, entries 2–6) and EWG (Table 1, entry 7) substituents did not affect the reaction yields in comparison to the reaction performed with unsubstituted thiophenol. Decylthiol was chosen to introduce long aliphatic chain into the structure (Table 1, entry 9). However, compound **2i** was obtained in a modest 37% yield. Introduction of other aliphatic thiols, such as benzyl mercaptan (Table 1, entry 8) and *N*-acetyl-*L*-cysteine methyl ester (Table 1, entry 10), resulted in better yields. Nevertheless, reactions performed with the aliphatic thiols occurred with lower yields than those with the aromatic ones. Formation of **2h–i** was monitored by ^{19}F NMR analysis. ^{31}P NMR spectra of crude material confirmed the full conversion of **1a**. However, lower yields which the reactions occurred with, were caused by formation of several minor by-

Table 1 Reaction conditions and yield of products formed in S_NAr reactions of **1a** with nucleophiles

Entry	Compound	Nucleophile	Conditions	Yield [%]
1	**2a**	C_6H_5SH	TRIS, DMF, rt, 2 h	87
2	**2b**	$4\text{-}CH_3C_6H_4SH$		89
3	**2c**	$3,5\text{-}(CH_3)_2C_6H_3SH$		81
4	**2d**	$4\text{-}CH_3OC_6H_4SH$		95
5	**2e**	$3\text{-}CH_3OC_6H_4SH$		84
6	**2f**	$3\text{-}NH_2C_6H_4SH$		76
7	**2g**	$4\text{-}BrC_6H_4SH$		86
8	**2h**	$C_6H_5CH_2SH$		65
9	**2i**	$CH_3(CH_2)_8CH_2SH$		37
10	**2j**	*N*-acetyl-L-cysteine methyl ester		71
11	**2k**	CH_3NH_2	DMSO, 80 °C, 3 h	71
12	**2l**	$CH_3(CH_2)_2NH_2$		74
13	**2m**	$CH_3(CH_2)_3NH_2$		60
14	**2n**	$CH_2{=}CHCH_2NH_2$		65
15	**2o**	$C_6H_5CH_2NH_2$		63
16	**2p**	C_6H_5OH	K_2CO_3, DMF, 80 °C, 24 h	68
17	**2q**	$4\text{-}CH_3OC_6H_4OH$		48
18	**2r**	$4\text{-}ClC_6H_4OH$		56
19	**2s**	$3\text{-}NO_2C_6H_4OH$		48

products. This can be rationalized by the fact that aliphatic thiols are better nucleophiles in comparison to thiophenols thus, their reactivity is increased.

Reaction of **1a** with a large excess of alkylamine in DMSO after 3 hours of heating at 80 °C gave aryl aminophosphonates **2k–o** in yields ranging from 60 to 74% (Table 1, entries 11–15). Progress of the reactions was monitored by ^{19}F NMR, and after 3 hours a total conversion of the starting α-aminophosphonate was generally observed.

Different phenols were consecutively used as nucleophiles. The expected products were obtained in moderate yields (Table 1, entry 16–19). Following known procedure for this kind of reactions,[42,43] the syntheses were performed in DMF in the presence of K_2CO_3, at 80 °C for 24 hours. In comparison to alcoxides in which the negative charge is located only on the oxygen atom, phenoxides are much softer nucleophiles therefore, the reactions proceeded efficiently.

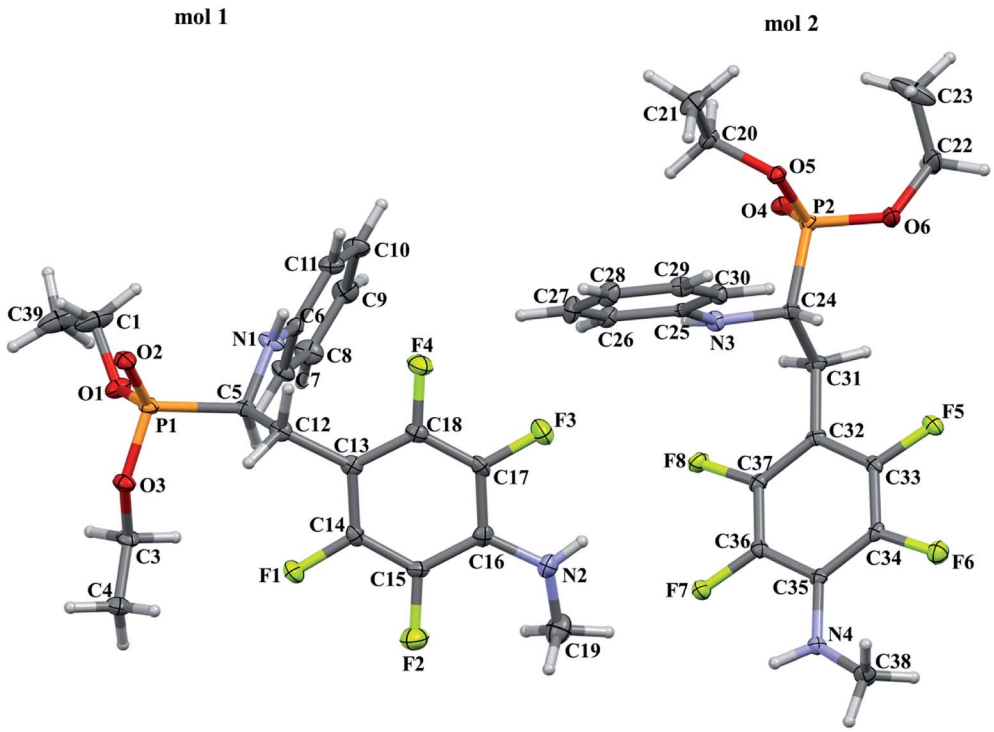

Fig. 1 A perspective view showing the asymmetric part of unit cell of **2k** together with the labelling atoms scheme. Ellipsoids are drawn at the 30% probability level, hydrogen atoms are represented by spheres of arbitrary radii.

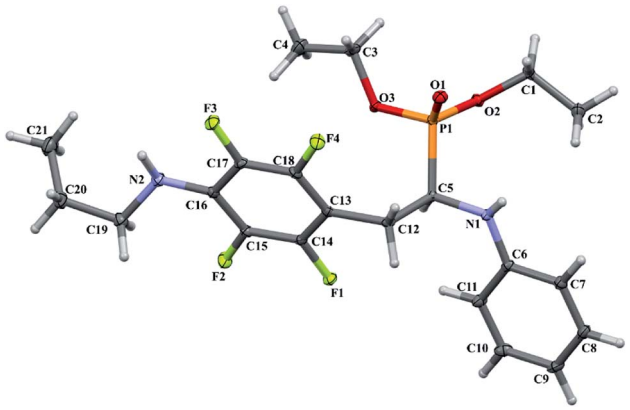

Fig. 2 A perspective view showing the asymmetric part of unit cell of **2l** together with the labelling atoms scheme. Ellipsoids are drawn at the 30% probability level, hydrogen atoms are represented by spheres of arbitrary radii.

2.2 X-ray and DFT studies

In order to comprehensively understand the structural features of compounds investigated we made attempts to grow their crystals by slow evaporation of toluene solutions under ambient conditions. This process resulted in obtaining crystals suitable for X-ray single crystal diffraction analysis only for **2k** and **2l**. In terms of chemistry, compounds **2k** and **2l** differ in the chain length of substituent in *para* position of the fluorinated ring; **2k** contains the methylamine group, while propylamine group is present in **2l**. Molecules of **2k** and **2l** are chiral, however, they are not enantiomerically pure since the racemic mixture of substrate (**1a**) was used for their synthesis. Thus, crystallization yielded single crystals containing both enantiomers. Since the nitrogen atoms included in the molecular structure of **2k** and **2l** are pyramidal in shape, *i.e.* are bonded to three different groups and possess lone pair of electrons, they constitute stereogenic centres. This, in turn, may affect the occurrence of diastereomers in the crystals.

Both compounds examined crystallize in the triclinic space group *P*-1. **2k** crystallizes with two molecules (mol 1 and mol 2) in the asymmetric unit that adopt a similar molecular conformation described by two torsion angles Csp^2–N–Csp^3–Csp^3 and Csp^2–Csp^3–Csp^3–N. The torsion angle values are −131.3(3)° and −83.9(3)° for mol 1, and 147.3(2)° and −68.9(3)° for mol 2, while the dihedral angle of two aromatic rings are 68.6(3)° and 78.0(3)° in mol 1 and 2, respectively. Adoption of very similar conformation (marked as a conformation B), by some phosphonates analogues of fluorophenylalanine was previously observed in our research group.[33] The main structural differences are displayed within the aliphatic diethyl phosphonate chains (Csp^3–Csp^3–O–P) where the chains adopt antiperiplanar–antiperiplanar conformation with the corresponding torsion angle values of −171(3) and 165.7(2)° for mol 1, while the synclinal–antiperiplanar conformation is characterized by the values of 65.5(4) and 176.1(2)° for mol 2. Interestingly, the configuration of the aniline nitrogen atom in both symmetrically independent molecules shows the opposite stereochemistry *i.e. S* in mol 1 and *R* in mol 2; however, the methylamine moieties have the same *R* configuration. As a consequence these two molecules possess *R*(C5), *S*(N1), *R*(N2) and *R*(C24), *R*(N3), *R*(N4) configurations, respectively. Therefore they are diastereomers. Since the crystals of **2k** are centrosymmetric, two pairs of diastereomers coexist in the crystal structure. The pyramidal environment of N atom in methylamine group also affects significant deviation of this group from the tetrafluorophenyl plane; the Csp^2–Csp^2–N–Csp^3 torsion angle is 18.6(5)° in mol 1 and 21.2(4)° in mol 2. In contrast, **2l** crystallizes with one molecule in the asymmetric unit and adopts previously described conformation C (extended)[33] with the corresponding torsion angles of 80.3(2)° and −172.4(2)°. The anticlinal–antiperiplanar combination of the aliphatic diethyl phosphonate chains have torsion angles of 107.5(2) and 178.8(2)°. The propylamine group adopts a folded conformation with an N–Csp^3–Csp^3–Csp^3 torsion angle of 62.5(3)°. The stereochemistry of nitrogen atoms in this group is *S* while in the aniline moiety is *R*, hence the molecule in the asymmetric unit has a *R*(C5), *R*(N1), *S*(N2) configuration. The crystals investigated were chosen such that the *R* stereogenic centre at the carbon atom constitutes the asymmetric unit. The molecular structures of **2k** and **2l** are shown in Fig. 1 and 2.

The different configuration exhibited by the aniline nitrogen atoms in **2k**, prompted us to use quantum-chemical methods to study energy differences between the diastereomers. For this purpose all possible stereomers (*R*,*R*,*R*; *R*,*S*,*S*; *R*,*S*,*R*; *R*,*R*,*R*) were built based on the geometry of mol 1 derived from the crystal. The calculations were performed *in vacuo*, as well as using the polarisable continuum model (PCM) to take into account the

Table 2 Relative energies (Δ*E* (kcal mol^{-1}))[a], zero-point energy (ZPE (kcal mol^{-1}))[b], thermal correction to Gibbs free energy (TCG (kcal mol^{-1}))[c] and percentage of populations (Pop) calculated for **2k** stereomers *in vacuo* and using PCM for chloroform at the WB97XD/6-31+G(d) level of theory. Not that the absolute configuration *R* is imposed at the C5 and C24 carbon atoms

Stereomer	Δ*E in vacuo*	Δ*E* in chloroform	ZPE	TCG	Pop *in vacuo*	Pop in chloroform
R,*S*,*R*	0.00	5.12	0.00	0.00	98.9	<1.0
R,*S*,*S*	2.35	5.25	0.15	0.50	1.0	<1.0
R,*R*,*S*	5.77	1.88	0.39	0.97	<1.0	20.2
R,*R*,*R*	5.90	0.00	0.78	2.00	<1.0	79.1

[a] Relative energies calculated with respect to the lowest energy structure at WB97XD/6-31+G(d) level is equal to −1813.40587669 hartree. [b] Zero-point energy; the lowest value was equal to 0.412559 hartree. [c] Thermal correction to Gibbs free energy at 298 K; the lowest value was equal to 0.348198 hartree. The relative energy in chloroform was equal to −1813.41658767 hartree.

Table 3 Valence angles values at nitrogen atoms in crystal structure of **2k** (X-ray), and calculated at the WB97XD/6-31+G(d) level of theory (DFT). The numbering of valence angles are the same as numbering atoms scheme in Fig. 1. Not that the absolute configuration *R* is imposed at the C5 and C24 carbon atoms

	Stereomer					
The valence angle [°]	*R*,*S*,*R* DFT	X-ray	*R*,*R*,*R* DFT	X-ray	*R*,*R*,*S* DFT	*R*,*S*,*S* DFT
C6–N1–H1 or C25–N3–H3	112.3	116.7	113.6	115.2	114.2	113.1
C5–N1–H1 or C24–N3–H3	113.2	115.8	112.3	117.1	113.1	113.3
C6–N1–C5 or C25–N3–C24	126.1	125.4	123.1	124.9	123.5	126.2
Sum of the valence angles	**351.6**	**357.9**	**349.0**	**357.2**	**350.8**	**352.6**
C16–N2–H2 or C35–N4–H4	111.6	115.9	111.1	113.9	111.5	111.5
C19–N2–H2 or C38–N4–H4	113.4	116.9	112.8	113.2	113.2	113.3
C16–N2–C19 or C35–N4–C38	121.8	125.2	120.7	123.3	121.6	121.5
Sum of the valence angles	**346.8**	**358.0**	**344.9**	**350.4**	**346.3**	**346.3**

effect of chloroform solution as NMR spectra of **2k** were recorded for the compound sample dissolved in $CDCl_3$.

The results obtained support structural diversity of the possible stereomers. The results show that the *R*,*R*,*R* stereomer is energetically favourable at WB97XD/6-31+G(d) level of theory including PCM, while *in vacuo* the lowest relative energy is assigned to the *R*,*S*,*R* stereomer (Table 2).

These findings suggest a strong influence of surrounding medium on the energy preferences of stereomers (diastereomers). *In vacuo* the *R*,*S*,*R* stereomer constitutes over 98% in the population of the calculated diastereomers (Table 2). Its population drops below 1% when chloroform solvent is taken into consideration *via* PCM approximation. In chloroform *R*,*R*,*R* stereomer seems to be predominant as it constitutes almost 80% in the population of diastereomers – a striking difference with its contribution (below 1%) *in vacuo*.

Analysis of the nitrogen atoms pyramidal environment in both the optimized and crystal structures of **2k** shows strong deviation from the ideal tetrahedral geometry, described by set of valence angles equal to 109.5°, towards the planar one. As

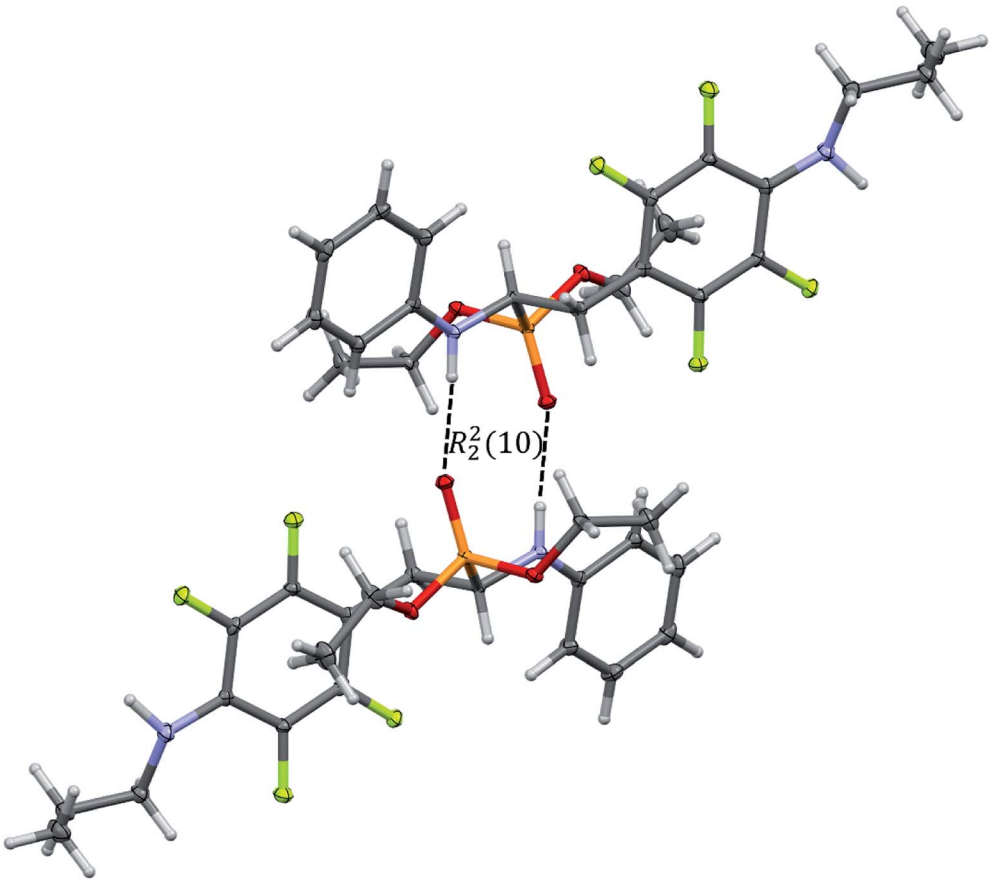

Fig. 3 Dimeric motif of N–H···O(=P) hydrogen bonds between two enantiomers of opposite stereochemistry in the crystals of **2l**. This motif is also observed in the crystals of **2k**.

Table 4 Geometrical parameters describing the N–H···O interactions in the crystals of **2k** and **2l**

	D–H [Å]	H···A [Å]	D···A [Å]	D–H···A [°]	SYMM
2k					
N1–H1···O1	0.81(2)	2.16(2)	2.975(3)	177(2)	$[-x+2, -y+1, -z+1]$
N3–H3···O4	0.86(2)	2.12(3)	2.964(2)	168(3)	$[-x+1, -y+1, -z]$
2l					
N1–H1···O1	0.85(3)	2.03(3)	2.871(3)	173(2)	$[-x+1, -y+2, -z+1]$

seen in Table 3, the valence angles values in both structures are similar. For example, in the crystal structure the values of C6–N1–H1, C5–N1–H1 and C6–N1–C5 valence angles are equal to 116.7°, 115.8°, and 125.4°, in mol 1, and 115.2°, 117.1°, and 124.9° for C25–N3–H3, C24–N3–H3 and C24–N3–C25 in mol 2, while in the calculated *R,R,R* stereomer the corresponding valence angles adopt values of 113.6°, 112.3° and 123.1° (Table 3). The sum of the valence angles values in the crystal structure is equal to 357.9° and 357.2°, in mol 1 and mol 2, respectively, and 349° in the *R,R,R* stereomer calculated. All these values correspond to forms between the ideally planar (360°) and ideally tetrahedral (328.5°) geometry but closer to the planar one.

The bond order analysis showed that bond order for the bond between C6–N1 (nitrogen atom attached to the carbon atom in the phenyl ring) is *ca* 1.10. For the bond between C16–N2 (nitrogen atom attached to the carbon atom in the perfluorinated phenyl ring) the bond order is *ca* 1.12, further explaining partially planar arrangement at the nitrogen atoms. Indeed the pyramidal shape at the N atom can invert its configuration in the structures investigated. The energy barrier of transition between the diastereomers (invertomers) was estimated in DFT calculations to *ca* 2.7 kcal mol^{-1} *in vacuo*. The temperature of coalescence (T_c) was approximated to *ca* 53 K in accordance to eqn (2) (Experimental section). The transition energy in chloroform differed from the value calculated *in vacuo* conditions, and was estimated to *ca* 2.5 kcal mol^{-1}. The T_c temperature was approximated to *ca* 50 K.

Our quantum chemical computational results refer to isolated molecule or a molecule in a polarisable continuum that model chloroform solution. On the other hand in the solid state the molecules can interact with the actual molecules in the crystal environment. Unfortunately, the attempt to perform calculations with PBC (Periodic Boundary Conditions) for such

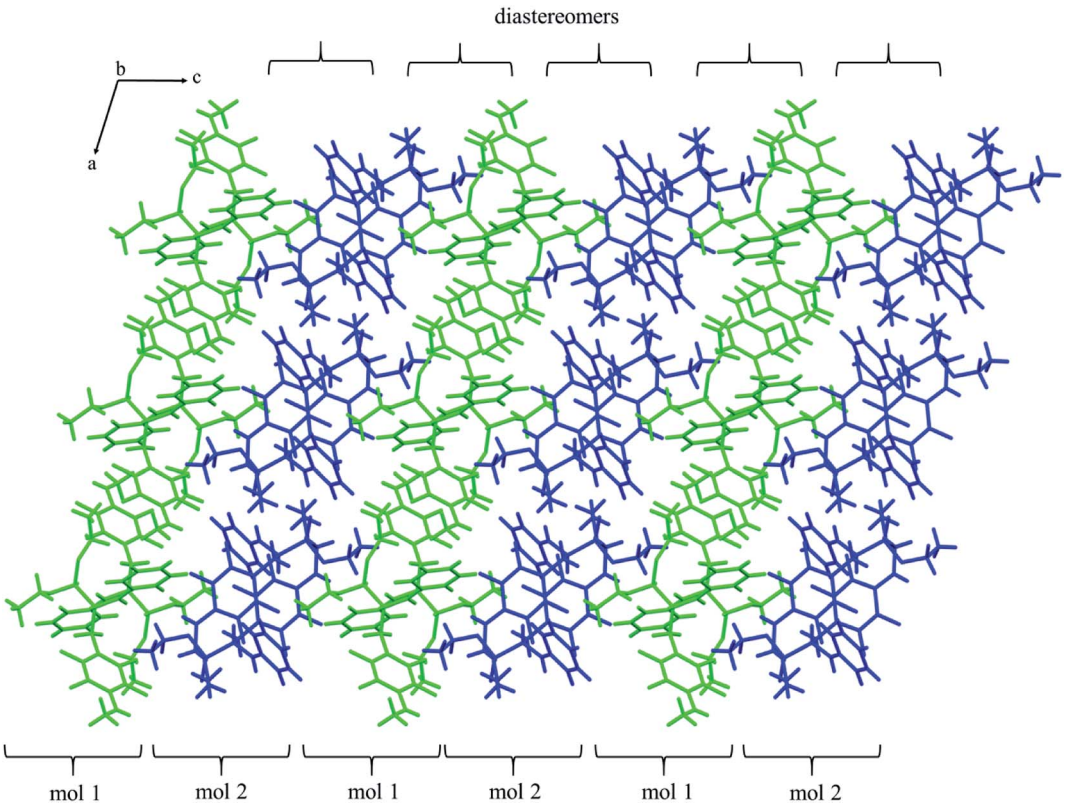

Fig. 4 Self-sorting of diastereomers on supramolecular level in the crystals of **2k**. Two symmetry independent molecules that represent two diastereomers (mol 1 and mol 2) were distinguished by green and blue colors.

Table 5 Geometrical parameters for other types of intermolecular interactions that occurs in the crystals investigated

	D–H [Å]	H···A [Å]	D···A [Å]	D–H···A [°]	SYMM
2k					
C11–H11···F7	0.95	2.55(3)	3.333(4)	140(3)	$[x + 1, y, z]$
C22–H22A···F3	0.99	2.55(3)	3.387(4)	143(3)	$[-x + 1, -y + 1, -z]$
C26–H26···F3	0.95	2.42(2)	3.153(3)	134(3)	
N4–H4···O1	0.85(3)	2.29(4)	3.074(3)	154(3)	$[-x + 1, -y + 1, -z + 1]$
N2–H2···F7	0.79(3)	2.53(3)	3.017(3)	121(3)	
C22–H22A···π	0.99	2.78(4)	3.486(5)	129(4)	$[-x + 1, -y + 1, -z]$
C22–H22B···π	0.99	2.67(5)	3.529(6)	145(5)	$[-x + 1, -y + 1, -z]$
C28–H28···F5	0.95	2.67(3)	3.299(3)	125(3)	$[-x, -y, -z]$
2l					
C1–H1B···F1	0.99	2.59(3)	3.339(2)	133(2)	$[-x + 2, -y + 2, -z + 1]$
C5–H5···O2	1.00	2.62(2)	3.526(2)	152(2)	$[-x + 2, -y + 2, -z + 1]$
N2–H2···F3	0.98(3)	2.19(3)	3.159(2)	171(2)	$[-x + 1, -y + 1, -z]$

a large system resulted in failure due to restrictions on supercomputer's resources.

In the crystal structures of **2k** and **2l** the principal interactions are N–H···O(=P) hydrogen bonds that hold two enantiomers of opposite stereochemistry together around a centre of symmetry, as shown in Fig. 3. Geometrical parameters describing hydrogen bonds are listed in Table 4. It is worth

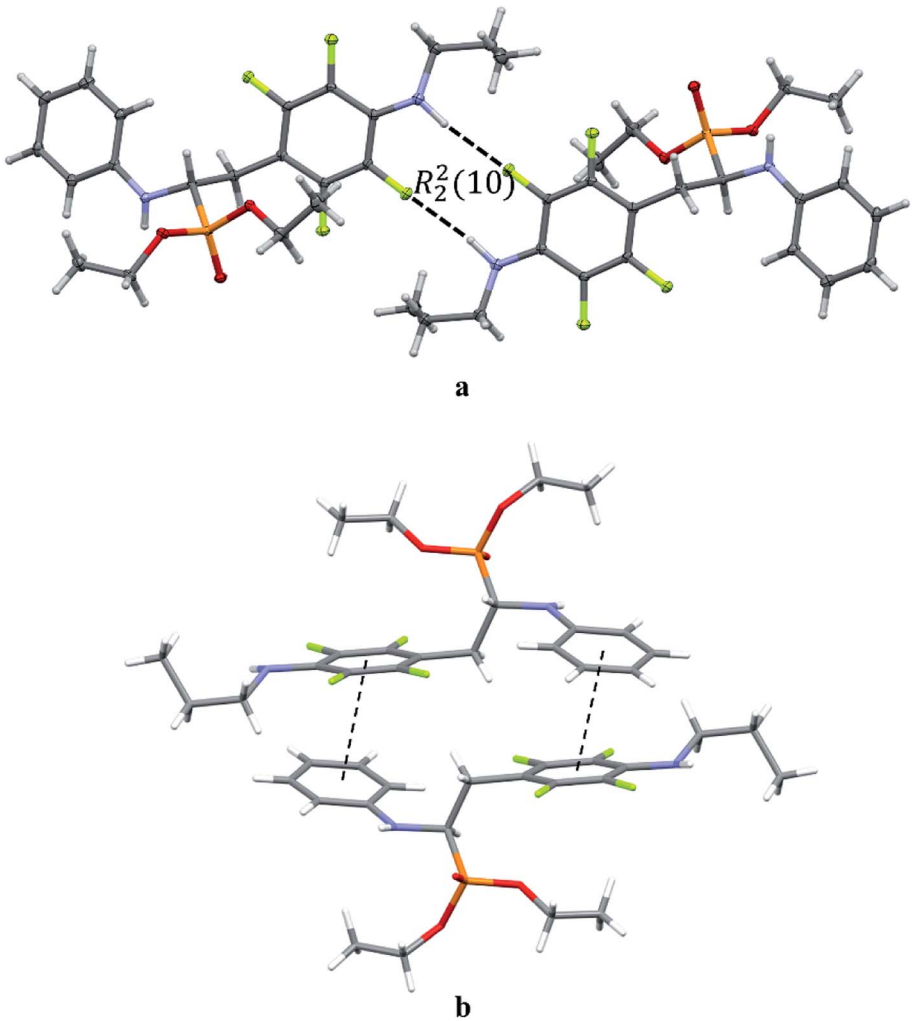

Fig. 5 Dimeric motif of N–H···F interactions (a) and π···π interactions between two enantiomers of opposite stereochemistry in the crystals of **2l** (b).

noting that in **2k** this motif occurs between enantiomers but not between diastereomers.

The self-sorting phenomenon of diastereomers at supramolecular level is observed in the crystals of **2k**. Since there are two diastereomers in the asymmetric unit, each of them forms separate layer perpendicular to *c* lattice direction containing pairs of enantiomers. The layers are stabilized by the previously mentioned N–H···O(=P) hydrogen bonds, which are supported by interactions involving π-electrons. The fluorinated rings of two neighbouring mol 1 oriented parallel to each other favours the formation of π···π interactions between these moieties, while a tilted arrangement of fluorinated and non-fluorinated aromatic rings of two mol 2 leads to formation of H···π and H···F contacts (2.77(3) and 2.67(3) Å, respectively) that are equal or shorter than the sum of van der Waals radii of hydrogen and carbon atoms (H_{vdW} = 1.2 Å, C_{vdW} = 1.7 Å, the sum = 2.9 Å),[45] and hydrogen and fluorine atoms (F_{vdWr} = 1.47 Å, the sum is 2.67 Å).[45] The geometrical parameters describing π···π interactions are 3.319(3) and 0.88 Å for distance between the planes of aromatic rings along with the offset, respectively. The two layer types are alternately arranged in the crystal as shown in Fig. 4, and are related to each other through N–H···O(=P) hydrogen bonds in which the methylamine group acts as a donor of hydrogen bonds. The geometrical parameters of the hydrogen bond listed in Table 5 suggest that the interactions between diastereomers are slightly weaker than those between enantiomers in the layer. Moreover, the proximity of the aromatic rings and ester group belonging to diastereomers in two neighbouring layers promotes the formation of multiple H···F and H···F interactions and thus substantially affects the crystal structure stabilization.

The extended C molecular conformation of **2l** favours self-association forming dimers in which the two molecules interact *via* N–H···F hydrogen bonding and strong affects the formation of isolated π···π intermolecular interactions between fluorinated and non-fluorinated aromatic rings as shown in Fig. 5. The interacting rings are tilted toward each other by 16° while the interplanar distance between the centres of gravity is 3.796 Å. The intermolecular interactions present in the crystals are reported in Table 5.

2.3 Biological evaluation

Six randomly chosen S_NAr reactions products, and also six of the fluorinated phosphonate analogues of phenylalanine, including **1a**, previously synthesized in our research group,[33] were subjected to biological studies. The first group of compounds contained mainly different thiophenols derivatives, while various α-aminophosphonates differing in number and position of fluorine substituents in one of the phenyl rings constituted the second group.

In the compounds molecules, apart from amino group, two additional pharmacophores are present; fluorine substituents and phosphonate group that replaced an amino acid carbonyl one. A considerable number of α-aminophosphonates is known to exhibit various biological activities including anticancer one. On the other hand, a lot of existing drugs, for example synthetic statins and 5-fluorouracil, contain fluorine. This shows a remarkable potential of fluorine in pharmaceutical chemistry and provide a source for drug discovery.[18] Therefore combination of fluorine pharmacophore with amino and phosphonate group in molecules of target compounds was expected to have an impact on their bioactivity.

2.3.1 Drug likeness. With the aim to develop novel antiproliferative therapeutics, which are orally bioavailable and focusing particularly on glioma treatment, human intestinal absorption and blood–brain barrier penetration of α-aminophosphonates were calculated. The structure-based prediction models depended on physiochemical and molecular properties of the compounds were performed with various computing software.

The most common criteria used for preliminary evaluation of drug likeness of a compound encompass the Lipinski's "rule of 5".[46,47] In this respect, the physicochemical parameters of the examined compounds generally match the rule (Table 6).

According to Veber's rule, reduced molecular flexibility, as measured by the number of rotatable bonds, and low polar surface area or total hydrogen bond count (sum of donors and

Table 6 Selected physicochemical data for the studies α-aminophosphonates[a]

Cpd	MW	aPSA [Å^2]	PSA [Å^2]	log *P*	HBD	HBA	RB	Caco-2 [nm s^{-1}]	BB	MDCK [nm s^{-1}]
1a	423.31	303.9	8.7	4.22	1	4	9	21.72	1.38	86.84
1b	385.80	294.6	13.5	4.27	1	4	9	21.79	1.30	102.26
1c	385.80	312.7	8.7	4.25	1	4	9	21.74	1.27	104.23
1d	383.37	295.7	13.5	4.18	1	4	9	21.72	1.26	116.53
1e	351.35	297.4	8.7	3.64	1	4	9	21.72	0.98	168.46
1f	387.34	283.1	13.5	3.95	1	4	9	21.72	1.00	109.96
2b	527.52	364.9	27	6.25	1	4	11	21.72	1.06	42.40
2d	543.52	363.8	35.3	5.75	1	5	12	21.72	0.18	12.35
2e	543.52	367.5	36	5.75	1	5	12	21.72	0.18	14.77
2f	528.51	325.4	52	5.18	3	5	11	21.70	0.19	3.94
2j	580.15	329.0	81.8	3.75	2	8	15	21.69	0.01	0.06
2r	531.87	361.8	13.4	5.92	1	5	11	21.73	3.06	44.20

[a] MW – molecular weight, aPSA – apolar surface area, PSA – polar surface area, log *P* – an octanol–water partition coefficient calculated with ALOGPS 2.1, HBD – number of hydrogen bond donors, HBA – number of hydrogen bond acceptors, RB – rotatable bonds number.

Table 7 Cytotoxicity (IC_{50}) values of the studies α-aminophosphonates

Compound	Compound structure	T98G IC_{50} [μM]	U-118 MG IC_{50} [μM]	HaCaT IC_{50} [μM]
1a	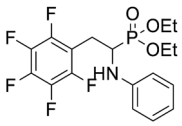	40.4 ± 6.2	60.67 ± 8.9	56.8 ± 7.4
1b	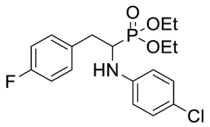	73.5 ± 9.2	88.2 ± 7.5	>100
1c	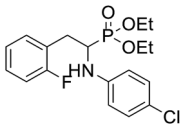	67.9 ± 11.2	91.2 ± 15.5	>100
1d	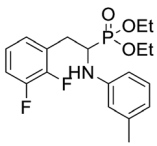	71.3 ± 8.7	48.6 ± 10.4	67.9 ± 11.8
1e	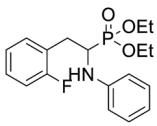	106.4 ± 14.7	86.8 ± 7.2	61.8 ± 9.1
1f	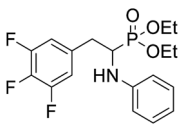	25.1 ± 4.5	40.8 ± 8.4	33.2 ± 5.1
2b	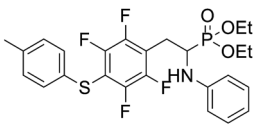	14.5 ± 3.3	37.9 ± 2.5	26.5 ± 4.7
2d	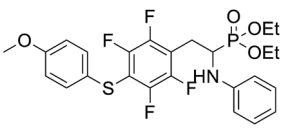	36.8 ± 5.7	33.2 ± 7.3	19.8 ± 3.9
2e	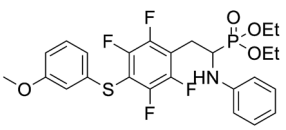	20.4 ± 3.1	21.4 ± 2.7	10.1 ± 2.2
2f	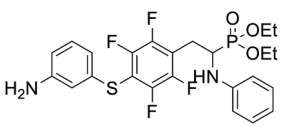	25.5 ± 1.9	28.1 ± 3.6	18.2 ± 3.4
2j	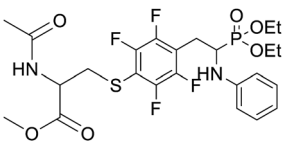	82.7 ± 15.7	>100	>100
2r	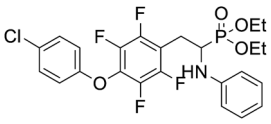	70.3 ± 8.3	79.2 ± 6.4	48.4 ± 7.4

Table 7 (*Contd.*)

Compound	Compound structure	T98G IC_{50} [μM]	U-118 MG IC_{50} [μM]	HaCaT IC_{50} [μM]
5-FdU (5-fluoro-2′-deoxyuridine)	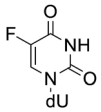	5.57 ± 0.9	23.40 ± 1.6	4.42 ± 1.1

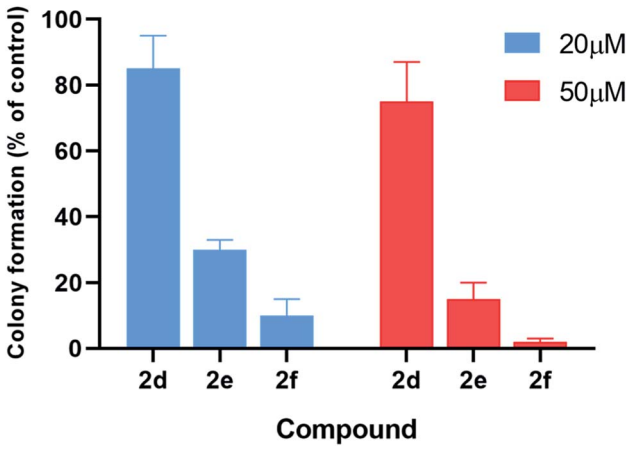

Fig. 6 Treatment with compounds **2d–f** significantly reduces the colony-forming ability of T98G cells as compared to untreated cells. Error bars display the standard deviation from at least three independent measurements.

acceptors) are found to be important predictors of good oral bioavailability, independent of molecular weight.[48] Veber's observations suggest that compounds which meet only the two criteria: 10 or fewer rotatable bonds and polar surface area equal to or less than 140 $Å^2$ (or 12 or fewer H-bond donors and acceptors) will have a high probability of good oral bioavailability. All of the examined compounds meet these criteria perfectly (Table 6).

Caco-2 cell permeability model classifies compounds into 3 classes of permeability (high, medium and low). Compounds with t_{Papp} below 4 nm s^{-1} are classified as low permeable; compounds with t_{Papp} above 70 nm s^{-1} are classified as high permeable and compounds with permeability values between 4–70 nm s^{-1} are classified as medium.[49] For blood–brain barrier penetration we calculated the BB value which is defined as the ratio of the concentration of a drug in the brain and in the blood, measured at equilibrium ($BB = C_{Brain}/C_{Blood}$). Compounds with BB > 2.0 cross the blood–brain barrier readily (high absorption to CNS (central nervous system)) while molecules with BB < 0.1 are poorly distributed to the brain (low absorption to CNS).[50] Results show that all compounds are characterized by a good intestinal absorption (20–80%) and relatively high brain penetration, therefore making these compounds more druggable (Table 6).

2.3.2 ***In vitro*** **cytostatic activity.** Two glioblastoma multiforme cell lines: T98G and U118 MG, and HaCaT as referential healthy cells were chosen. For comparison, IC_{50} values reflecting inhibitory activity of known anticancer drug 5-fluoro-2′-deoxyuridine in the chosen cell lines were included in Table 7.

As shown in this table, all compounds exhibited moderate cytostatic activity in the both glioblastoma cell lines. Most of the compounds showed higher activity against T98G cell line. Only **1d**, **1e** and to a small degree also **2d** occurred to be better inhibitors of U-118MG cell line. Most of the studied S_NAr reactions products displayed significantly higher inhibitory activity against both glioblastoma multiforme cell lines than the parent α-aminophosphonate **1a**. This indicates that the introduction of thiophenols, but not aliphatic thiols nor phenols, to the *para* position in the fluorinated phenyl ring of **1a** molecule improve the antiglioma activity. IC_{50} values also demonstrate that for compounds **2b**, **2d**, **2e** and **2f**, the substituents in the thiophenol moiety had an influence on the cytotoxic activity (Table 7). All these substituents belong to EDG and it can be concluded that less electrodonating character of CH_3 group than of OCH_3 and NH_2 groups, results in higher activity of **2b** in comparison with **2d–2f**. Among the S_NAr reactions products studied, **2b** exhibiting the highest cytotoxic activity against T98G cell line and good selectivity can be considered as the best candidate for antiglioma drug.

Analysis of IC_{50} values for α-aminophosphonates **1a–1f**, indicates that number of fluorine substituents in one aromatic ring as well as presence and character of substituents in the second ring contribute to the anticancer activity displayed by these compounds. Compounds **1b** and **1c** containing one fluorine and one chlorine atoms, exhibit very similar inhibitory activity against both cancer cell lines indicating that position of this fluorine atom does not influence much the activity. Comparing these compounds with the **1e** demonstrates that chlorine substituent may constitute an important factor contributing to anticancer activity. Number of fluorine substituents also seems to have impact on the cytotoxic inhibition, though the influence is irregular.

The inhibitory effects of α-aminophosphonates in T98G cells were further assessed by performing clonogenic assays (Fig. 6). Compounds **2d–f** were also significantly more potent than other compounds in this assay. Treatment with 20 μM **2d–f** resulted in clonogenic survival of 85%, 30%, and 10%, respectively, compared to control cells. When we tested the effect of each compound at 50 μM, we found that **2d** reduces cancer cell clonogenic potential by 25%, **2e** by 85%, and **2f** by 98%.

3. Conclusions

Several diethyl (2-(perfluorophenyl)-1-(phenylamino)ethyl) phosphonate derivatives were synthesised by S_NAr reactions, and subjected to structural and biological studies. X-ray single crystal diffraction analysis performed for two of the obtained compounds (**2k** and **2l**) revealed their conformational preferences, self-sorting at supramolecular level and different conformation at the aniline nitrogen atoms. It was found that in the solid state, **2k** molecules adopt conformation with almost perpendicular arrangement of both aromatic rings, while molecule of **2l** prefers extended conformation with the aromatic rings arranged nearly parallel. Interestingly, in the crystals of parent **1a** its molecules also adopt conformation with parallel oriented rings. This indicates that introduction of substituent into *para* position in the fluorinated ring may or may not change the conformation of the resulted molecule comparing to the starting material.

Due to the different configuration at the aniline nitrogen atoms, two molecules in **2k** crystal structure constitute a pair of diastereomers. This phenomenon was studied with the use of quantum-chemical methods. Results obtained at WB97XD/6-31+G(d) level of theory for isolated molecule show energetic preference of *R*,*S*,*R* stereomer, while for a molecule in a polarisable continuum mimicking chloroform solution indicate the *R*,*R*,*R* stereomer as an energetically favourable. These results generally support the stereomers structural diversity. Coexistence of both stereomers observed in the crystal structure is most likely due to intermolecular interactions.

Structurally various α-aminophosphonates are known to exhibit activity against different cancer cell lines. However, to the best of our knowledge there is no studies referring to α-aminophosphonates as potential antiglioma agents. Malignant gliomas remain almost always fatal, and none of the current state of the art treatments can be regarded as effective.[51,52] Synthesised by S_NAr reactions phosphono-perfluorophenylalanine derivatives perfectly meet the criteria of Lipinski's and Veber's rules. MTT assay results demonstrated that the compounds, particularly these formed by introduction of thiophenol moiety to *para* position in the fluorinated ring, exhibited significantly higher inhibitory activity against T98G and U118 MG cell lines than the parent **1a**. This enables to conclude that phosphono-perfluorophenylalanine core constitute promising scaffold for further studies focused on developing of new agents active against glioblastoma multiforme.

4. Experimental Section

4.1 Synthesis

4.1.1 General methods. Reagent grade chemicals were used. Solvents were dried over 4 Å molecular sieves. All moisture sensitive reactions were carried out under nitrogen atmosphere with dry, freshly distilled reagents when possible. All glassware was carefully dried under vacuum with a flameless heat gun. TLC was performed on Merck Kieselgel 60-F254 with EtOAc/cyclohexane as eluent, and products were detected by UV light (254 nm) and with a solution of potassium permanganate. Merck Kieselgel 60 (230–400 mesh) was used for column chromatography. NMR spectra were recorded with instrument operating at 400 MHz (^{1}H), 101 MHz (^{13}C), 377 (^{19}F) and 162 MHz (^{31}P). Chemical shifts (δ) are given in ppm and calibrated from residual signals of $CDCl_3$ (7.26 ppm), acetone-d_6 (2.09 ppm) for ^{1}H NMR and $CDCl_3$ (77.16 ppm) and acetone-d_6 (29.84 ppm) for ^{13}C NMR. High resolution mass spectra were measured using electrospray ionization (ESI, positive-ion mode).

4.1.2 General procedure for the nucleophilic aromatic substitution of 1a with thiols. To the mixture of thiol (0.24 mmol) and tris(hydroxymethyl)aminomethane (0.037 g, 0.30 mmol) in dry DMF (1 mL), a solution of **1a** (0.05 g, 0.12 mmol) in dry DMF (1 mL) was added under N_2 atmosphere. The mixture was stirred at room temperature for 2 h. Then solvent was removed under vacuum, and the crude was purified by column chromatography (CH_2Cl_2/acetone 4 : 1, v/v).

*4.1.2.1 Diethyl (1-(phenylamino)-2-(2,3,5,6-tetrafluoro-4-(phenylthio)phenyl)ethyl)phosphonate (**2a**).* Pale yellow oil (48 mg, 87%). ^{1}H NMR (400 MHz, acetone-d_6): δ = 7.33–7.28 (m, 3H, 3 CHar), 7.18–7.16 (m, 2H, 2CHar), 7.06–7.02 (m, 2H, 2CHar), 6.70 (d, J = 7.9 Hz, 2H, 2CHar), 6.60 (t, J = 7.3 Hz, 1H, CHar), 4.86–4.83 (m, 1H, NH) 4.16–4.05 (m, 5H, 2OCH$_2$, CH), 3.36–3.30 (m, 1H, ArCH$_2$), 3.24–3.14 (m, 1H, ArCH$_2$), 1.25 (t, J = 7.1 Hz, 3H, CH$_3$), 1.20 (t, J = 7.1 Hz, 3H, CH$_3$). ^{19}F NMR (377 MHz, acetone-d_6) δ = −135.96 to −136.06 (m, 2F), −142.90 to −142.99 (m, 2F). ^{31}P NMR (162 MHz, acetone-d_6) δ = 22.95 (s). ^{13}C NMR (101 MHz, $CDCl_3$) δ = 148.05–145.45 (m, 2Car) 146.31 (d, J = 7.3 Hz, Car), 146.79–144.11 (m, 2Car) 133.39 (s, Car), 129.83 (s, 2CHar), 129.32–129.26 (m, 4 CHar) 127.50 (s, CHar), 118.77 (s, CHar), 118.25–117.89 (m, Car), 113.28 (s, 2CHar), 112.14–111.74 (m, Car), 63.73 (d, J = 7.0 Hz, OCH$_2$), 62.46 (d, J = 7.4 Hz, OCH$_2$), 50.46 (d, J = 158.3 Hz, CH), 25.16 (d, J = 7.4 Hz, ArCH$_2$), 16.56, 16.51, 16.45, and 16.39 (2CH$_3$). HRMS (ESI$^+$) calcd for $C_{24}H_{25}F_4NO_3PS$ (M + H)$^+$: 514.1229, found: 514.1230.

*4.1.2.2 Diethyl (1-(phenylamino)-2-(2,3,5,6-tetrafluoro-4-(m-tolylthio)phenyl)ethyl)phosphonate (**2b**).* Pale yellow solid (55 mg, 89%), mp = 103–105 °C. ^{1}H NMR (400 MHz, acetone-d_6) δ = 7.20–7.10 (m, 4H, 4 CHar), 7.05–7.01 (m, 2H, 2CHar), 6.70 (d, J = 7.9 Hz, 1H, 2CHar), 6.60 (t, J = 7.3 Hz, 1H, CHar), 4.87–4.83 (m, 1H, NH), 4.13–4.04 (m, 5H, CH, 2OCH$_2$), 3.33–3.28 (m, 1H, ArCH$_2$), 3.22–3.13 (m, 1H, ArCH$_2$), 2.30 (s, 3H, ArCH$_3$), 1.24 (t, J = 7.1 Hz, 3H, CH$_3$), 1.19 (t, J = 7.1 Hz, 3H, CH$_3$). ^{19}F NMR (377 MHz, $CDCl_3$) δ = −134.05 (dd, J = 23.6, 11.5 Hz, 2F), −142.52 to −142.62 (m, 2F). ^{31}P NMR (162 MHz, acetone-d_6) δ = 23.01 (s). ^{13}C NMR (101 MHz, $CDCl_3$) δ = 147.96–146.36 (m, 2Car), 146.77–144.05 (m, 2Car), 146.32 (d, J = 7.2 Hz, Car), 137.99 (s, Car), 130.83 (s, 2CHar), 130.11 (s, 2CHar), 129.62 (s, Car), 129.31 (s, 2CHar), 118.80 (s, CHar), 117.83–117.47 (m, Car), 113.36 (s, 2CHar), 112.87 (s, Car), 63.75 (d, J = 7.0 Hz, OCH$_2$), 62.48 (d, J = 7.4 Hz, OCH$_2$), 50.51 (d, J = 158.2 Hz, CH), 25.13 (d, J = 7.4 Hz, ArCH$_2$), 21.23 (s, ArCH$_3$), 16.59, 16.54, 16.48, and 16.42 (2CH$_3$). HRMS (ESI$^+$) calcd for $C_{25}H_{27}F_4NO_3PS$ (M + H)$^+$: 528.1385, found: 528.1387.

*4.1.2.3 Diethyl (2-(4-((3,5-dimethylphenyl)thio)-2,3,5,6-tetrafluorophenyl)-1-(phenylamino)ethyl)phosphonate (**2c**).* Pale yellow solid (52 mg, 81%). ^{1}H NMR (400 MHz, acetone-d_6) δ =

7.05–7.01 (m, 2H, 2CHar), 6.91–6.89 (m, 3H, 3 CHar), 6.72 (d, J = 7.8 Hz, 2H, 2CHar), 6.57 (t, J = 7.3 Hz, 1H, CHar), 4.89–4.86 (m, 1H, NH), 4.13–4.02 (m, 5H, CH, $2OCH_2$), 3.33–3.30 (m, 1H, $ArCH_2$), 3.23–3.13 (m, 1H, $ArCH_2$), 2.83 (s, 6H, 2 $ArCH_3$), 1.23 (t, J = 7.1 Hz, 3H, CH_3), 1.17 (t, J = 7.1 Hz, 3H, CH_3). ^{19}F NMR (377 MHz, $CDCl_3$) δ = −133.72 to −133.81 (m, 2F), −142.38 (dd, J = 24.4, 11.9 Hz, 2F). ^{31}P NMR (162 MHz, acetone-d_6) δ = 23.10 (s). ^{13}C NMR (101 MHz, $CDCl_3$) δ = 148.13–145.45 (m, 2Car), 146.78–144.11 (m, 2Car) 146.30 (d, J = 6.5 Hz, Car), 139.06 (s, Car), 132.63 (s, 2Car), 129.69 (s, CHar) 129.31 (s, 2CHar), 128.05 (s, 2CHar), 118.87 (s, CHar), 118.13–117.64 (m, Car), 113.49 (s, 2CHar), 112.67–112.26 (m, Car), 63.69 (d, J = 7.0 Hz, OCH_2), 62.44 (d, J = 7.4 Hz, OCH_2), 50.60 (d, J = 157.4 Hz, CH), 25.09 (d, J = 7.3 Hz, $ArCH_2$), 21.28 (s, 2 $ArCH_3$), 16.56, 16.51, 16.44, and 16.38 ($2CH_3$). HRMS (ESI^+) calcd for $C_{26}H_{29}F_4NO_3PS$ $(M + H)^+$: 542.1542, found: 542.1542.

*4.1.2.4 Diethyl (1-(phenylamino)-2-(2,3,5,6-tetrafluoro-4-((-methoxyphenyl)thio)phenyl)ethyl)phosphonate (**2d**).* Pale yellow solid (61 mg, 95%), mp = 93–95 °C. ^{1}H NMR (400 MHz, acetone-d_6) δ = 7.30–7.28 (m, 2H, 2CHar), 7.05–6.98 (m, 2H, 2CHar), 6.92–6.90 (m, 2H, 2CHar), 6.68 (d, J = 7.8 Hz, 2H, 2CHar), 6.58 (t, J = 7.2 Hz, 1H, CHar), 4.85–4.82 (m, 1H, NH), 4.11–4.06 (m, 5H, CH, $2OCH_2$), 3.80 (s, 3H, $ArCH_3$), 3.31–3.27 (m, 1H, $ArCH_2$), 3.19–3.10 (m, 1H, $ArCH_2$), 1.23 (t, J = 7.1 Hz, 3H, CH_3), 1.17 (t, J = 7.1 Hz, 3H, CH_3). ^{19}F NMR (377 MHz, $CDCl_3$) δ = −134.67 (dd, J = 24.0, 11.8 Hz, 2F), −142.70 (dd, J = 24.3, 12.2 Hz, 2F). ^{31}P NMR (162 MHz, acetone-d_6) δ = 23.04 (s). ^{13}C NMR (101 MHz, $CDCl_3$): δ = 159.95 (s, Car), 147.79–145.13 (m, 2Car), 146.70–144.00 (m, 2Car), 146.30 (d, J = 7.1 Hz, Car), 134.07 (s, 2CHar), 129.25 (s, 2CHar), 123.25 (s, Car), 118.74 (s, CHar), 117.61–117.11 (m, Car), 114.88 (s, 2CHar), 114.14–113.69 (m, Car), 113.36 (s, 2CHar), 63.69 (d, J = 7.0 Hz, OCH_2), 62.43 (d, J = 7.4 Hz, OCH_2), 55.44 (s, OCH_3), 50.47 (d, J = 158.1 Hz, CH), 25.00 (s, $ArCH_2$), 16.54, 16.49, 16.42, 16.36 ($2CH_3$). HRMS (ESI^+) calcd for $C_{25}H_{27}F_4NO_4PS$ $(M + H)^+$: 544.1335, found: 544.1339.

*4.1.2.5 Diethyl (1-(phenylamino)-2-(2,3,5,6-tetrafluoro-4-((3-methoxyphenyl)thio)phenyl)ethyl)phosphonate (**2e**).* Yellow oil (61 mg, 95%). ^{1}H NMR (400 MHz, acetone-d_6) δ = 7.23 (t, J = 8.0 Hz, 1H, CHar), 7.06–7.02 (m, 2H, 2CHar), 6.85–6.80 (m, 2H, 2CHar), 6.71 (d, J = 7.9 Hz, 1H, 2CHar), 6.66 (d, J = 7.9 Hz, 1H, CHar), 6.59 (t, J = 7.3 Hz, 1H, CHar), 4.88–4.86 (m, NH), 4.15–4.04 (m, 5H, $2OCH_2$, CH), 3.75 (s, 3H, OCH_3), 3.36–3.30 (m, 1H, $ArCH_2$), 3.24–3.14 (m, 1H, $ArCH_2$), 1.25 (t, J = 7.1 Hz, 3H, CH_3), 1.19 (t, J = 7.0 Hz, 3H, CH_3). ^{19}F NMR (377 MHz, $CDCl_3$): δ = −133.45 to −133.55 (m, 2F), −142.22 (dd, J = 24.4, 12.4 Hz, 2F). ^{31}P NMR (162 MHz, acetone-d_6): δ = 23.04 (s). ^{13}C NMR (101 MHz, $CDCl_3$): δ = 159.99 (s, Car), 148.10–145.44 (m, 2Car), 147.90–144.05 (m, 2Car), 146.28 (d, J = 6.9 Hz, Car), 134.52 (s, Car), 130.15 (s, CHar), 129.28–129.24 (s, 2CHar), 121.84 (s, CHar), 118.81 (s, CHar), 118.40–118.04 (m, Car), 115.25 (s, CHar), 113.34 (s, 2CHar), 113.12 (s, CHar), 111.88–111.47 (m, Car), 63.68 (d, J = 7.0 Hz, OCH_2), 62.45 (d, J = 7.4 Hz, OCH_2), 55.34 (s, OCH_3), 50.48 (d, J = 157.9 Hz, CH), 25.12 (d, J = 7.3 Hz, $ArCH_2$), 16.53, 16.47, 16.42, and 16.36 ($2CH_3$). HRMS (ESI^+) calcd for $C_{25}H_{27}F_4NO_4PS$ $(M + H)^+$: 544.1335, found: 544.1328.

*4.1.2.6 Diethyl (2-(4-((3-aminophenyl)thio)-2,3,5,6-tetrafluorophenyl)-1-(phenylamino)ethyl)phosphonate (**2f**).* Pale yellow oil (47 mg, 76%). ^{1}H NMR (400 MHz, acetone-d_6) δ = 7.06–6.96 (m, 3H, 3 CHar), 6.71 (d, J = 8.3 Hz, 2H, 2CHar), 6.57 (m, 3H, 3 CHar), 6.35 (d, J = 8.2 Hz, 1H, CHar), 4.86–4.83 (m, 1H, NH_2), 4.76–4.74 (m, 1H, NH_2), 4.13–4.06 (m, 6H, CH, NH_2OCH_2), 3.35–3.29 (m, 1H, $ArCH_2$), 3.23–3.14 (m, 1H, $ArCH_2$), 1.24 (t, J = 7.1 Hz, 3H, CH_3), 1.19 (t, J = 7.1 Hz, 3H, CH_3). ^{19}F NMR (377 MHz, $CDCl_3$) δ = −133.46 (dd, J = 23.5, 11.4 Hz, 2F), −142.32 to −142.42 (m, 2F). ^{31}P NMR (162 MHz, acetone-d_6) δ = 23.04 (s). ^{13}C NMR (101 MHz, $CDCl_3$) δ = 148.19–145.53 (m, 2Car), 147.21 (s, Car), 146.65–144.08 (m, 2Car), 146.35 (d, J = 6.6 Hz, Car), 134.31 (s, Car), 130.12 (s, CHar), 129.35 (s, 2CHar), 119.61 (s, CHar), 118.80 (s, CHar), 118.37–117.88 (m, Car), 115.64 (s, CHar), 114.24 (s, CHar), 113.41 (s, 2CHar), 112.18–111.78 (m, Car), 63.68 (d, J = 7.0 Hz, OCH_2), 62.51 (d, J = 7.4 Hz, OCH_2), 50.56 (d, J = 157.9 Hz, CH), 25.09 (s, $ArCH_2$), 16.58, 16.52, 16.47, and 16.42 ($2CH_3$). HRMS (ESI^+) calcd for $C_{24}H_{26}F_4N_2O_3PS$ $(M + H)^+$: 529.1338, found: 529.1335.

*4.1.2.7 Diethyl (2-(4-((4-bromophenyl)thio)-2,3,5,6-tetrafluorophenyl)-1-(phenylamino)ethyl)phosphonate (**2g**).* Pale yellow solid (60 mg, 86%), mp = 77–79 °C. ^{1}H NMR (400 MHz, acetone-d_6) δ = 7.52–7.49 (m, 2H, 2CHar), 7.14–7.04 (m, 2H, 2CHar), 7.05–7.04 (m, 2H, 2CHar), 6.70 (d, J = 8.6 Hz, 2H, 2CHar), 6.61 (t, J = 7.4 Hz, 1H, CHar), 4.87–4.83 (m, 1H, NH), 4.16–4.05 (m, 5H, CH, $2OCH_2$), 3.36–3.29 (m, 1H, $ArCH_2$), 3.24–3.18 (m, 1H, $ArCH_2$), 1.26 (t, J = 7.1 Hz, 3H, CH_3), 1.20 (t, J = 7.0 Hz, 3H, CH_3). ^{19}F NMR (377 MHz, acetone-d_6) δ = −135.90 to −136.00 (m, 2F), −142.59 to −142.69 (m, 2F). ^{31}P NMR (162 MHz, acetone-d_6) δ = 22.89 (s). ^{13}C NMR (101 MHz, $CDCl_3$) δ = 148.05–145.38 (m, 2Car), 146.87–144.21 (m, 2Car) 146.33 (d, J = 7.2 Hz, Car), 132.59 (s, Car), 132.46 (s, 2CHar), 131.50 (s, 2CHar), 129.34 (s, 2CHar), 121.74 (s, Car), 118.79 (s, CHar), 118.49 (s, Car), 113.27 (s, 2CHar), 111.45 (s, Car), 63.78 (d, J = 7.0 Hz, OCH_2), 62.54 (d, J = 7.4 Hz, OCH_2), 50.43 (d, J = 158.6 Hz, CH), 25.23 (d, J = 7.5 Hz, $ArCH_2$), 16.61, 16.56, 16.51, and 16.45 ($2CH_3$). HRMS (ESI^+) calcd for $C_{24}H_{24}BrF_4NO_3PS$ $(M + H)^+$: 592.0334, found: 592.0336.

*4.1.2.8 Diethyl (2-(4-(benzylthio)-2,3,5,6-tetrafluorophenyl)-1-(phenylamino)ethyl)phosphonate (**2h**).* Yellow oil (40 mg, 65%). ^{1}H NMR (400 MHz, acetone-d_6) δ = 7.33–7.20 (m, 1H, CHar), 7.17 (s, 4H, 4 CHar), 7.08–7.04 (m, 2H, 2CHar), 6.70 (d, J = 7.9 Hz, 2H, 2CHar), 6.59 (t, J = 7.3 Hz, 1H, CHar), 4.82–4.79 (m, 1H, NH), 4.13–4.02 (m, 7H, SCH_2, CH, $2OCH_2$), 3.30–3.24 (m, 1H, $ArCH_2$), 3.17–3.08 (m, 1H, $ArCH_2$), 1.24 (t, J = 7.1 Hz, 3H, CH_3), 1.17 (t, J = 7.1 Hz, 3H, CH_3). ^{19}F NMR (377 MHz, acetone-d_6) δ = −136.30 to −136.40 (m, 2F), −143.81 to −143.90 (m, 2F). ^{31}P NMR (162 MHz, acetone-d_6) δ = 23.13 (s). ^{13}C NMR (101 MHz, $CDCl_3$) δ = 148.18–145.53 (m, 2Car), 146.48–143.90 (m, 2Car) 146.45 (d, J = 5.7 Hz, Car), 136.55 (s, Car), 129.32 (s, 2CHar), 128.85 (s, CHar), 128.66 (s, 2CHar), 127.75 (s, 2CHar), 118.81 (s, CHar), 117.27–116.91 (m, Car), 113.51 (s, 2CHar), 112.49–112.08 (m, Car), 63.59 (d, J = 7.0 Hz, OCH_2), 62.45 (d, J = 7.4 Hz, OCH_2), 50.62 (d, J = 157.1 Hz, CH), 39.14 (s, $ArCH_2S$), 24.93 (d, J = 6.9 Hz, $ArCH_2$), 16.56, 16.51, 16.48, and 16.42 ($2CH_3$). HRMS (ESI^+) calcd for $C_{25}H_{27}F_4NO_3PS$ $(M + H)^+$: 528.1385, found: 528.1387.

*4.1.2.9 Diethyl (2-(4-(decylthio)-2,3,5,6-tetrafluorophenyl)-1-(phenylamino)ethyl)phosphonate (**2i**).* Yellow oil (25 mg, 36%).

^{1}H NMR (400 MHz, $CDCl_3$) δ = 7.07–7.03 (m, 2H, 2CHar), 6.64 (t, J = 7.3 Hz, 1H, CHar), 6.53 (d, J = 7.9 Hz, 2H, 2CHar), 4.18–4.01 (m, 5H, CHP, 2OCH$_2$), 3.82–3.79 (m, 1H, NH), 3.28–3.24 (m, 1H, ArCH$_2$), 3.17–3.14 (m, 1H, ArCH$_2$), 2.80 (t, J = 7.3 Hz, 2H, CH$_2$S), 1.48–1.19 (m, 22H, 2CH$_3$, CH$_3$(CH$_2$)$_8$), 0.88 (t, J = 6.9 Hz, 3H, CH$_3$(CH$_2$)$_9$). ^{19}F NMR (377 MHz, $CDCl_3$) δ = −134.89 (dd, J = 24.3, 12.0 Hz, 2F), −143.26 (dd, J = 24.3, 12.1 Hz, 2F). ^{31}P NMR (162 MHz, $CDCl_3$) δ = 23.52 (s). ^{13}C NMR (101 MHz, $CDCl_3$) δ = 148.15–145.53 (m, 2Car), 146.68–143.97 (m, 2Car) 146.41 (d, J = 6.9 Hz, Car), 129.27 (s, 2CHar), 118.76 (s, CHar), 116.81–116.44 (m, Car), 113.44 (s, 2CHar), 113.15 (s, Car), 63.67 (d, J = 7.0 Hz, OCH$_2$), 62.46 (d, J = 7.4 Hz, OCH$_2$), 50.61 (d, J = 157.7 Hz, CH), 34.84 (s, SCH$_2$), 32.01 (s, CH$_3$(CH$_2$)$_8$), 29.83 (s, CH$_3$(CH$_2$)$_8$), 29.63 (s, CH$_3$(CH$_2$)$_8$), 29.59 (s, CH$_3$(CH$_2$)$_8$), 29.41 (s, CH$_3$(CH$_2$)$_8$), 29.16 (s, CH$_3$(CH$_2$)$_8$), 28.48 (s, CH$_3$(CH$_2$)$_8$), 25.03 (d, J = 7.3 Hz, ArCH$_2$), 22.80 (s, CH$_3$(CH$_2$)$_8$), 16.59, 16.53, 16.49, and 16.43 (2CH$_3$), 14.23 (s, CH$_3$(CH$_2$)$_9$) ppm. HRMS (ESI$^+$) calcd for $C_{28}H_{41}F_4NO_3SP$ (M + H)$^+$: 578.2481, found: 578.2477.

*4.1.2.10 Methyl 2-acetamido-3-((4-(2-(diethoxyphosphoryl)-2-(phenylamino)ethyl)-2,3,5,6-tetrafluorophenyl)thio) propanoate (**2j**).* Yellow oil (49 mg, 71%). ^{1}H NMR (400 MHz, $CDCl_3$) δ = 7.06 (t, J = 7.7 Hz, 2H, 2CHar), 6.65 (t, J = 7.2 Hz, 1H, CHar), 6.54–6.51 (m, 2H, 2CHar), 6.38–6.34 (m, 1H, NHCO), 4.76–4.72 (m, 1H, CHN), 4.14–4.08 (m, 5H, CHP, 2OCH$_2$), 3.86, 3.85 (2d, J = 3.6, 3.6 Hz, 1H, ArNH), 3.44, 3.41 (2s, 3H, CH$_3$O), 3.35–3.14 (m, 4H, ArCH$_2$, SCH$_2$), 1.92 (s, 3H, CH$_3$CO), 1.29 (t, J = 7.1 Hz, 3H, CH$_3$), 1.17 (td, J = 7.1, 3.4 Hz, 3H, CH$_3$). ^{19}F NMR (377 MHz, $CDCl_3$) δ = −133.64 to −133.74 (m, 2F), −142.36 to −142.49 (m, 2F) ppm. ^{31}P NMR (162 MHz, $CDCl_3$): δ = 23.45 and 23.41 (2s). ^{13}C NMR (101 MHz, $CDCl_3$) δ = 170.28 (s, CO), 169.92, 169.90 (2s, CO), 148.16–145.56 (m, 2Car), 146.31, 146.29 (2d, J = 5.0, 4.8 Hz, Car), 145.71–144.24 (m, 2Car), 129.34 (s, 2CHar), 118.86, 118.83 (2s, CHar), 118.10–117.59 (m, Car), 113.51, 113.44 (2s, 2CHar), 111.81–111.40 (m, Car), 63.6 (d, J = 7.0 Hz, POCH$_2$), 62.56, 62.48 (2d, J = 7.5, 7.4 Hz, POCH$_2$), 52.56, 52.55 (2s, CH$_3$O), 52.08, 52.02 (2s, CHCH$_2$S), 50.5, 50.4 (2d, J = 156.1, 156.2 PCH), 36.31, 36.24 (2t, J = 2.2, 2.1 Hz, SCH$_2$), 24.89, 24.82 (2d, J = 5.1, 6.2 Hz, ArCH$_2$), 22.95 (s, COCH$_3$), 16.5, 16.4 (2d, J = 5.3, 5.7 Hz, CH$_3$). HRMS (ESI$^+$) calcd for $C_{24}H_{30}F_4N_2O_6PS$ (M + H)$^+$: 581.1498, found: 581.1503.

4.1.3 General procedure for the nucleophilic aromatic substitution of 1a with amines. To the mixture of **1a** (0.05 g, 0.12 mmol) in dry DMSO (1 mL), amine (3.6 mmol) was added under N_2 atmosphere in a Radley's tube. The mixture was stirred at 80 °C for 3 h. After cooling to the room temperature, the reaction mixture was poured into water (10 mL) and Et_2O (10 mL). The aqueous phase was extracted with Et_2O (3 × 10 mL), then combined organic layers were washed with water (3 × 20 mL) and dried over $MgSO_4$. After filtration, solvent was removed under reduced pressure and the crude was purified by column chromatography (cyclohexane/AcOEt 1 : 1, v/v).

*4.1.3.1 Diethyl (1-(phenylamino)-2-(2,3,5,6-tetrafluoro-4-(methylamino)phenyl)ethyl)phosphonate (**2k**).* Pale yellow solid (31 mg, 60%), mp = 74–76 °C. ^{1}H NMR (400 MHz, $CDCl_3$) δ = 7.10–7.06 (m, 2H, 2CHar), 6.65 (t, J = 7.4 Hz, 1H, CHar), 6.55 (d, J = 7.9 Hz, 2H, 2CHar), 4.17–3.97 (m, 5H, CH, 2OCH$_2$), 3.77 (dd, J = 10.6, 3.4 Hz, 1H, NH), 3.66 (bs, 1H, NH), 3.19–3.13 (m, 1H, ArCH$_2$), 3.06–2.99 (m, 4H, NCH$_3$, ArCH$_2$), 1.30 (t, J = 7.0 Hz, 3H, CH$_3$), 1.20 (t, J = 7.1 Hz, 3H, CH$_3$). ^{19}F NMR (377 MHz, $CDCl_3$) δ = −146.46 to −146.55 (m, 2F), −161.22 to −161.30 (m, 2F). ^{31}P NMR (162 MHz, $CDCl_3$) δ = 24.13 (s). ^{13}C NMR (101 MHz, $CDCl_3$) δ = 147.18–144.46 (m, 2Car), 146.75 (d, J = 5.9 Hz, Car), 138.76–136.11 (m, 2Car), 129.22 (s, 2CHar), 124.77–124.68 (m, Car), 118.42 (s, CHar), 113.48 (s, 2CHar), 103.17–102.67 (m, Car), 63.44 (d, J = 7.0 Hz, OCH$_2$), 62.34 (d, J = 7.5 Hz, OCH$_2$), 51.06 (d, J = 156.3 Hz, CH), 33.18 (s, NCH$_3$), 24.03 (d, J = 6.6 Hz, ArCH$_2$), 16.60, 16.55, 16.52, 16.46 (2CH$_3$). HRMS (ESI$^+$) calcd for $C_{19}H_{24}F_4N_2O_3P$ (M + H)$^+$: 435.1461, found: 435.1465.

*4.1.3.2 Diethyl (1-(phenylamino)-2-(2,3,5,6-tetrafluoro-4-(propylamino)phenyl)ethyl)phosphonate (**2l**).* Pale yellow solid (40 mg, 74%), mp = 78–80 °C. ^{1}H NMR (400 MHz, $CDCl_3$) δ = 7.08–7.04 (m, 1H, 2CHar), 6.64 (t, J = 7.3 Hz, 1H, CHar), 6.54 (d, J = 7.9 Hz, 2H, 2CHar), 4.17–3.98 (m, 5H, CH, 2OCH$_2$), 3.80–3.65 (m, 1H, NH), 3.65 (s, 1H, CH$_2$NH), 3.27–3.22 (m, 2H, CH$_3$CH$_2$-CH$_2$N), 3.18–3.13 (m, 1H, ArCH$_2$), 3.06–3.00 (m, 1H, ArCH$_2$), 1.52 (dd, J = 14.4, 7.2 Hz, 2H, CH$_3$CH$_2$CH$_2$N), 1.30 (t, J = 7.1 Hz, 3H, CH$_3$), 1.20 (t, J = 7.1 Hz, 3H, CH$_3$), 0.92 (t, J = 7.4 Hz, 3H, CH$_3$CH$_2$CH$_2$N). ^{19}F NMR (377 MHz, $CDCl_3$) δ = −146.46 to −146.53 (m, 2F), −160.68 to −160.72 (m, 2F). ^{31}P NMR (162 MHz, $CDCl_3$) δ = 24.13 (s). ^{13}C NMR (101 MHz, $CDCl_3$) δ = 147.16–144.51 (m, 2Car), 146.72 (d, J = 6.3 Hz, Car), 138.79–136.16 (m, 2Car), 129.17 (s, 2CHar) 127.17–126.90 (m, Car), 118.37 (s, CHar), 113.42 (s, 2CHar), 103.16–102.64 (m, Car), 63.45 (d, J = 7.0 Hz, OCH$_2$), 62.31 (d, J = 7.5 Hz, OCH$_2$), 51.03 (d, J = 156.8 Hz, CH), 47.82 (t, J = 4.0 Hz, CH$_3$CH$_2$CH$_2$N), 24.04 (d, J = 7.0 Hz, ArCH$_2$), 23.93 (s, CH$_3$CH$_2$CH$_2$N), 16.57, 16.52, 16.49, and 16.43 (2CH$_3$), 11.17 (s, CH$_3$CH$_2$CH$_2$N). HRMS (ESI$^+$) calcd for $C_{21}H_{28}F_4N_2O_3P$ (M + H)$^+$: 463.1774, found: 463.1773.

*4.1.3.3 Diethyl (2-(4-(butylamino)-2,3,5,6-tetrafluorophenyl)-1-(phenylamino)ethyl)phosphonate (**2m**).* Yellow oil (40 mg, 71%). ^{1}H NMR (400 MHz, $CDCl_3$) δ = 7.06 (t, J = 7.9 Hz, 2H, 2CHar), 6.64 (t, J = 7.3 Hz, 1H, CHar), 6.54 (d, J = 7.9 Hz, 2H, 2CHar), 4.17–3.97 (m, 5H, CH, 2OCH$_2$), 3.78 (dd, J = 10.8, 3.1 Hz, 1H, NH), 3.60 (bs, 1H, NH), 3.31–3.25 (m, 2H, NCH$_2$), 3.18–3.13 (m, 1H, ArCH$_2$), 3.06–3.00 (m, 1H, ArCH$_2$), 1.49–1.28 (m, 7H, CH$_3$, CH$_2$CH$_2$), 1.20 (t, J = 7.1 Hz, 3H, CH$_3$), 0.92 (t, J = 7.3 Hz, 3H, CH$_3$(CH$_2$)$_3$). ^{19}F NMR (377 MHz, $CDCl_3$) δ = −146.45 to −146.52 (m, 2F), −160.68 to −160.72 (m, 2F). ^{31}P NMR (162 MHz, $CDCl_3$) δ = 24.13 (s) ppm. ^{13}C NMR (101 MHz, $CDCl_3$) δ = 147.16–146.70 (m, 2Car), 146.73 (d, J = 6.2 Hz, Car), 138.77–136.15 (m, 2Car), 129.18 (s, 2CHar) 127.20–126.97 (m, Car) 118.38 (s, CHar) 113.43 (s, 2CHar) 103.13–102.61 (m, Car) 63.45 (d, J = 7.0 Hz, OCH$_2$), 62.31 (d, J = 7.5 Hz, OCH$_2$), 51.05 (d, J = 156.8 Hz, CH), 45.82 (t, J = 4.0 Hz, NCH$_2$), 32.88 (s, CH$_2$CH$_2$-CH$_2$), 24.04 (d, J = 6.7 Hz, ArCH$_2$), 19.88 (s, CH$_3$CH$_2$CH$_2$), 16.58, 16.52, 16.49, and 16.43 (2CH$_3$), 13.87 (s, CH$_3$(CH$_2$)$_3$). HRMS (ESI$^+$) calcd for $C_{22}H_{30}F_4N_2O_3P$ (M + H)$^+$: 477.1930, found: 477.1932.

*4.1.3.4 Diethyl (2-(4-(allylamino)-2,3,5,6-tetrafluorophenyl)-1-(phenylamino)ethyl)phosphonate (**2n**).* Pale yellow oil (35 mg, 65%). ^{1}H NMR (400 MHz, $CDCl_3$) δ = 7.09–7.05 (m, 2H, 2CHar), 6.64 (t, J = 7.3 Hz, 1H, CHar), 6.54 (d, J = 7.9 Hz, 2H, 2CHar), 5.88–5.81 (m, 1H, CH$_2$=CH), 5.15 (ddd, J = 13.7, 11.5, 1.3 Hz, 2H, CH$_2$=CH), 4.17–4.02 (m, 5H, CHP, 2OCH$_2$), 3.89–3.88 (m,

2H, NCH_2), 3.77–3.76 (m, 2H, 2 NH), 3.20–3.14 (m, 1H, $ArCH_2$), 3.07–2.97 (m, 1H, $ArCH_2$), 1.30 (t, J = 7.1 Hz, 3H, CH_3), 1.20 (t, J = 7.1 Hz, 3H, CH_3). ^{19}F NMR (377 MHz, $CDCl_3$) δ = −146.13 to −146.22 (m, 2F), −159.83 to −159.92 (m, 2F). ^{31}P NMR (162 MHz, $CDCl_3$) δ = 24.08 (s). ^{13}C NMR (101 MHz, $CDCl_3$) δ = 147.14–146.66 (m, 2Car), 146.70 (d, J = 6.3 Hz, Car), 138.93–136.29 (m, 2Car), 135.27 (s, CH_2=CH), 129.20 (s, 2CHar), 126.66–126.39 (m, Car), 118.42 (s, CHar), 116.86 (s, CH_2=CH), 113.43 (s, 2CHar), 103.89–103.38 (m, Car), 63.50 (t, J = 6.8 Hz, OCH_2), 62.37 (t, J = 8.9 Hz, OCH_2), 51.01 (d, J = 156.8 Hz, CHP), 48.35 (t, J = 4.3 Hz, NCH_2), 24.09 (d, J = 7.0 Hz, $ArCH_2$), 16.58, 16.52, 16.49, 16.43 ($2CH_3$). HRMS (ESI^+) calcd for $C_{21}H_{26}F_4N_2O_3P$ $(M + H)^+$: 461.1617, found: 461.1616.

*4.1.3.5 Diethyl (1-(phenylamino)-2-(2,3,5,6-tetrafluoro-4-(methylamino)phenyl)ethyl)phosphonate (**2o**).* Pale yellow oil (38 mg, 63%). ^{1}H NMR (400 MHz, acetone-d_6) δ = 7.33–7.27 (m, 5H, 5 CHar), 7.04–7.00 (m, 2H, 2CHar), 6.67–6.65 (m, 2H, 2CHar), 6.57 (t, J = 7.3 Hz, 1H, CHar), 5.60 (bs, 1H, $NHCH_2$), 4.71–4.67 (m, 1H, NH), 4.52 (d, J = 7.0 Hz, 2H, NCH_2), 4.08–4.01 (m, 5H, CH, $2OCH_2$), 3.16–3.10 (m, 1H, $ArCH_2$), 3.00–2.90 (m, 1H, $ArCH_2$), 1.21 (t, J = 7.1 Hz, 3H, CH_3), 1.15 (t, J = 7.0 Hz, 3H, CH_3). ^{19}F NMR (377 MHz, acetone-d_6) δ = −147.27 to −147.39 (m, 2F), −161.21 to −161.32 (m, 2F). ^{31}P NMR (162 MHz, acetone-d_6) δ = 23.69 (s). ^{13}C NMR (101 MHz, $CDCl_3$): δ = 146.91–144.51 (m, 2Car), 146.69 (d, J = 6.0 Hz, Car), 139.10 (s, Car), 138.95–136.33 (m, 2Car), 129.23 (s, 2CHar), 128.89 (s, 2CHar), 127.81 (s, CHar), 127.67 (s, 2CHar), 126.72–126.57 (m, Car), 118.45 (s, CHar), 113.47 (s, 2CHar), 104.00–103.63 (m, Car), 63.47 (d, J = 7.0 Hz, OCH_2), 62.33 (d, J = 7.5 Hz, OCH_2), 51.01 (d, J = 156.0 Hz, CH), 50.18 (s, $ArCH_2N$), 24.09 (d, J = 7.1 Hz, $ArCH_2$), 16.58, 16.53, 16.49, 16.43 (2 × CH_3). HRMS (ESI^+) calcd for $C_{25}H_{28}F_4N_2O_3P$ $(M + H)^+$: 511.1774, found: 511.1774.

4.1.4 General procedure for the nucleophilic aromatic substitution of 1a with phenols. To the mixture of phenol (0.18 mmol) and K_2CO_3 (0.025 g, 0.18 mmol) in dry DMF (1 mL), a solution of **1a** (0.05 g, 0.12 mmol) in dry DMF (1 mL) was added under N_2 atmosphere in a Radley's tube. The mixture was stirred at 80 °C for 24 h. After cooling to the room temperature, the reaction mixture was poured into water (10 mL) and Et_2O (10 mL). The aqueous phase was extracted with Et_2O (3 × 10 mL), then combined organic layers were washed with water (3 × 20 mL) and dried over $MgSO_4$. After filtration, solvent was removed under reduced pressure and the crude was purified by column chromatography (cyclohexane/AcOEt 1 : 1, v/v).

*4.1.4.1 Diethyl (1-(phenylamino)-2-(2,3,5,6-tetrafluoro-4-phenoxyphenyl)ethyl)phosphonate (**2p**).* Yellow oil (40 mg, 68%). ^{1}H NMR (400 MHz, $CD_3C(O)CD_3$) δ = 7.39–7.35 (m, 2H, 2CHar), 7.17–7.10 (m, 1H, CHar), 7.07–7.05 (m, 2H, 2CHar), 6.81 (d, J = 8.2 Hz, 2H, 2CHar), 6.72 (d, J = 7.9 Hz, 2H, 2CHar), 6.65 (t, J = 7.3 Hz, 1H, CHar), 4.84–4.82 (m, 1H, NH), 4.19–4.09 (m, 5H, CH, $2OCH_2$), 3.33–3.30 (m, 1H, $ArCH_2$), 3.21–3.12 (m, 1H, $ArCH_2$), 1.29 (t, J = 7.1 Hz, 3H, CH_3), 1.22 (t, J = 7.2 Hz, 3H, CH_3). ^{19}F NMR (377 MHz, $CDCl_3$) δ = −143.74 to −143.83 (m, 2F), −154.95 to −155.03 (m, 2F). ^{31}P NMR (162 MHz, $CD_3C(O)CD_3$) δ = 23.02 (s). ^{13}C NMR (101 MHz, $CDCl_3$) δ = 157.27 (s, Car), 147.14–144.45 (m, 2Car), 146.50 (d, J = 8.0 Hz, Car), 142.77–140.05 (m, 2Car) 132.48–132.17 (m, Car), 129.83 (s, 2CHar), 129.37 (s, 2CHar), 123.61 (s, CHar), 118.66 (s, CHar), 115.38 (s, 2CHar), 113.17 (s, 2CHar), 112.74–112.23 (m, Car), 63.82 (d, J = 7.0 Hz, OCH_2), 62.55 (d, J = 7.4 Hz, OCH_2), 50.53 (d, J = 159.1 Hz, CH), 24.75 (d, J = 7.8 Hz, $ArCH_2$), 16.63, 16.57, 16.55 and 16.49 ($2CH_3$). HRMS (ESI^+) calcd for $C_{24}H_{25}F_4NO_4P$ $(M + H)^+$: 498.1457, found: 498.1459.

*4.1.4.2 Diethyl (1-(phenylamino)-2-(2,3,5,6-tetrafluoro-4-(4-methoxyphenoxy)phenyl)ethyl)phosphonate (**2q**).* Yellow solid (30 mg, 48%), mp = 97–99 °C. ^{1}H NMR (400 MHz, $CD_3C(O)CD_3$) δ = 7.08–7.01 (m, 2H, 2CHar), 6.92–6.88 (m, 2H, 2CHar), 6.78–6.76 (m, 2H, 2CHar), 6.72–6.69 (m, 2H, 2CHar), 6.65 (t, J = 7.4 Hz, 1H, CHar), 4.83–4.80 (m, 1H, NH), 4.16–4.09 (m, 5H, CH, $2OCH_2$), 3.78 (s, 3H, OCH_3), 3.33–3.27 (m, 1H, $ArCH_2$), 3.19–3.10 (m, 1H, $ArCH_2$), 1.30–1.26 (m, 3H, CH_3), 1.24–1.15 (m, 3H, CH_3). ^{19}F NMR (377 MHz, $CDCl_3$) δ = −143.91 to −144.00 (m, 2F), −155.33 to −155.42 (m, 2F). ^{31}P NMR (162 MHz, $CDCl_3$) δ = 23.42 (s). ^{13}C NMR (101 MHz, $CDCl_3$) δ = 155.85 (s, Car), 151.42 (s, Car), 147.13–144.49 (m, 2Car) 146.51 (d, J = 7.9 Hz, Car), 142.78–140.10 (m, 2Car), 133.40–133.04 (m, Car) 129.36 (s, 2CHar), 118.64 (s, CHar), 116.70 (s, 2CHar), 114.79 (s, 2CHar), 113.21 (s, 2CHar), 112.34–111.83 (m, Car), 63.80 (d, J = 7.0 Hz, OCH_2), 62.55 (d, J = 7.4 Hz, OCH_2), 55.82 (s, OCH_3), 50.57 (d, J = 158.7 Hz, CH), 24.70 (d, J = 7.6 Hz, $ArCH_2$), 16.63, 16.58, 16.55, and 16.50 ($2CH_3$). HRMS (ESI^+) calcd for $C_{25}H_{27}F_4NO_5P$ $(M + H)^+$: 528.1563, found: 528.1567.

*4.1.4.3 Diethyl (2-(4-(4-chlorophenoxy)-2,3,5,6-tetrafluorophenyl)-1-(phenylamino)ethyl)phosphonate (**2r**).* Yellow solid (35 mg, 56%), mp = 94–99 °C. ^{1}H NMR (400 MHz, $CD_3C(O)CD_3$) δ = 7.40–7.38 (m, 2H, 2CHar), 7.08–7.02 (m, 2H, 2CHar), 6.85–6.83 (m, 2H, 2CHar), 6.72 (d, J = 7.9 Hz, 2H, 2CHar), 6.66 (t, J = 7.3 Hz, 1H, CHar), 4.87–4.83 (m, 1H, NH), 4.17–4.10 (m, 5H, CH, $2OCH_2$), 3.34–3.28 (m, 1H, $ArCH_2$), 3.21–3.14 (m, 1H, $ArCH_2$), 1.29 (t, J = 7.1 Hz, 3H, CH_3), 1.22 (t, J = 7.1 Hz, 3H, CH_3). ^{19}F NMR (377 MHz, $CDCl_3$) δ = −143.37 to −143.45 (m, 2F), −154.94 to −155.02 (m, 2F). ^{31}P NMR (162 MHz, $CDCl_3$) δ = 23.24 (s). ^{13}C NMR (101 MHz, $CDCl_3$) δ = 155.79 (s, Car), 147.12–142.57 (m, 2Car), 146.47 (d, J = 8.1 Hz, Car), 142.57–139.85 (m, 2Car) 132.10–131.84 (m, Car), 129.77 (s, 2CHar), 129.36 (s, 2CHar), 128.73 (s, Car), 118.59 (s, CHar), 116.75 (s, 2CHar), 113.07 (s, 2CHar), 112.95–112.80 (m, Car), 63.87 (d, J = 7.0 Hz, OCH_2), 62.59 (d, J = 7.5 Hz, OCH_2), 50.38 (d, J = 159.4 Hz, CH), 24.74 (d, J = 7.9 Hz, $ArCH_2$), 16.62, 16.57, 16.55, and 16.49 ($2CH_3$) ppm. HRMS (ESI^+) calcd for $C_{24}H_{24}ClF_4NO_4P$ $(M + H)^+$: 532.1068, found: 532.1066.

*4.1.4.4 Diethyl (1-(phenylamino)-2-(2,3,5,6-tetrafluoro-4-(3-nitrophenoxy)phenyl)ethyl)phosphonate (**2s**).* Yellow solid (31 mg, 48%), mp = 77–79 °C. ^{1}H NMR (400 MHz, $CD_3C(O)CD_3$) δ = 8.05 (ddd, J = 8.2, 2.1, 0.8 Hz, 1H, CHar), 7.84 (t, J = 2.3 Hz, 1H, CHar), 7.71 (t, J = 8.3 Hz, 1H, CHar), 7.24 (dd, J = 8.3, 2.6 Hz, 1H, CHar), 7.10–7.06 (m, 2H, 2CHar), 6.74 (d, J = 7.9 Hz, 2H, 2CHar), 6.63 (t, J = 7.3 Hz, 1H, CHar), 4.86 (d, J = 13.7 Hz, 1H, NH), 4.17–4.10 (m, 5H, CH, $2OCH_2$), 3.35–3.30 (m, 1H, $ArCH_2$), 3.23–3.14 (m, 1H, $ArCH_2$), 1.28 (t, J = 7.1 Hz, 3H, CH_3), 1.22 (t, J = 7.1 Hz, 3H, CH_3). ^{19}F NMR (377 MHz, $CDCl_3$) δ = −142.44 (dd, J = 22.6, 9.4 Hz, 2F), −154.52 to −154.61 (dd, J = 22.0, 9.3 Hz, 2F). ^{31}P NMR (162 MHz, $CDCl_3$) δ = 23.25 (s). ^{13}C NMR (101 MHz, $CDCl_3$) δ = 157.42 (s, Car), 149.36 (s, Car),

147.24–144.60 (m, 2Car), 146.42 (d, J = 7.7 Hz, Car), 142.42–139.69 (m, 2Car), 131.44–130.97 (m, Car), 130.67 (s, CHar), 129.41 (s, 2CHar), 121.39 (s, CHar), 118.79 (s, CHar), 118.74 (s, CHar), 113.97–113.75 (m, Car), 113.28 (s, 2CHar), 111.18 (s, CHar), 63.83 (d, J = 7.0 Hz, OCH_2), 62.60 (d, J = 7.4 Hz, OCH_2), 50.47 (d, J = 158.6 Hz, CH), 24.85 (d, J = 7.8 Hz, $ArCH_2$), 16.63, 16.58, 16.55, and 16.50 ($2CH_3$). HRMS (ESI^+) calcd for $C_{24}H_{24}F_4N_2O_6P$ $(M + H)^+$: 543.1308, found: 543.1312.

4.2 X-ray and DFT studies

4.2.1 Crystal structure determination. Reflection intensities for crystals investigated were measured on Xcalibur diffractometer (Eos detector) equipped with a graphite monochromator and MoKa radiation (λ = 0.71073 Å). Data reduction and analysis were carried out with the CrysAlisPro software. In single-crystal experiments, the temperature of the crystals was controlled with an Oxford Instruments Cryosystem cold nitrogen-gas blower and was 100 K. The structures were solved by direct methods using SHELXS[53] and refined by the full-matrix least-squares techniques with SHELXL.[53] All heavy atoms were refined anisotropically. The hydrogen atoms bound to carbon atoms were placed at calculated positions and refined using a riding model. The positions of the amine H atoms were located reliably on difference Fourier maps and their position and displacement parameters were refined. Graphical images were produced in Mercury[54] programs.

*4.2.1.1 Crystals of **2k**.* $C_{19}H_{23}F_4N_2O_3P$, M_r = 434.36, 0.35 × 0.21 × 0.18 mm^3, triclinic, space group $P\bar{1}$ (no. 2), a = 11.7691(9) Å, b = 12.2935(5) Å, c = 16.8735(9) Å, α = 101.120(4)°, β = 99.040(5)°, γ = 118.147(6)°, V = 2023.5(2) $Å^3$, Z = 4, D_x = 1.426 g cm^{-3}, $F000$ = 904, MoK_α radiation, λ = 0.71073 Å, T = 100(2) K, $2\theta_{max}$ = 57.01°, 15 277 reflections collected, 8589 unique (R_{int} = 0.027), Final GooF = 1.028, R_1 = 0.0527, wR_2 = 0.1144, R indices based on 6237 with $I > 2\sigma(I)$ (refinement on F^2), 545 parameters, μ = 0.195 mm^{-1}.

*4.2.1.2 Crystals of **2l**.* $C_{21}H_{27}F_4N_2O_3P$, M_r = 462.41, 0.56 × 0.46 × 0.18 mm^3, triclinic, space group $P\bar{1}$ (no. 2), a = 8.8604(4) Å, b = 9.8978(8) Å, c = 13.1171(7) Å, α = 91.889(5)°, β = 91.350(4)°, γ = 109.119(6)°, V = 1085.59(12) $Å^3$, Z = 2, D_x = 1.415 g cm^{-3}, $F000$ = 484, MoK_α radiation, λ = 0.71073 Å, T = 100(2) K, $2\theta_{max}$ = 56.88°, 8189 reflections collected, 4658 unique (R_{int} = 0.0249), Final GooF = 1.040, R_1 = 0.0447, wR_2 = 0.0951, R indices based on 3666 with $I > 2\sigma(I)$ (refinement on F^2), 291 parameters, μ = 0.186 mm^{-1}, CCDC 1912530 and 1912531 contain the supplementary crystallographic data for this paper.

4.2.2 Computational methods. The calculations were performed *in vacuo*, as well as using the polarisable continuum model (PCM) to take into account the effect of chloroform solution as NMR spectra for **2k** were recorded for the compound sample dissolved in $CDCl_3$. The structures were optimized at the WB97XD[55] level and basis set with diffuse and polarization functions namely 6-31+G(d)[56–58] being a difficult compromise between the desired accuracy and computational time needed. The vibrational analyses were performed at the same level of theory. All calculations were carried out with the Gaussian 09 program suite[59] Boltzmann formalism,[60] and the percent of the structure Pop was computed according to the equation

$$\%\ \mathrm{Pop} = \frac{\exp(-\Delta G_x/RT)}{\sum_i \exp(-\Delta G_i/RT)} \times 100\% \quad (1)$$

The temperature for interconversion between possible stereomers was calculated on the basis of NMR studies using Earing's equation modified by Shanan-Atidi and Bar-Eli[61]

$$\Delta G = 4.57 T_c\{10.62 + \log[X/2\pi(1 - \Delta P)] + \log(T_c/\Delta v)\} \quad (2)$$

where ΔP = 0.04 and X = 1.636 as suggested for similar system.[62]

The relative energies of stereomers calculated at WB97XD/6-31+G(d) level of theory are summarized in Table 2.

4.3 Biological evaluation

4.3.1 Cell lines and culture conditions. Glioblastoma multiforme cell lines (T98G and U-118 MG), and non-cancerous cell line (HaCaT) were purchased from ATCC and CLS (Manassas, USA; Eppelheim, Germany). All cell lines are from human origin. U-118 MG were cultured in DMEM medium. T98G and HaCaT were cultured in EMEM medium. Each medium was supplemented with 10% fetal bovine serum (FBS) and 10 mg mL^{-1} antibiotics (penicillin and streptomycin). Cells were cultured at 37 °C with 5% CO_2 in humidified air. Cell media and other chemicals were obtained from Sigma-Aldrich Chemie GmbH (Steinheim, Germany) and ATCC. Cell concentrations in culture were adjusted to allow for exponential growth.

4.3.2 Cell viability/proliferation assay. Cell viability/proliferation was evaluated with a dye staining method using 3-(4,5-dimethyl-2-thiazolyl)-2,5-diphenyl-2*H*-tetrazolium bromide (MTT). The protocol is adapted from literature methods.[63] The monolayer cell culture was trypsinized and counted. To each well of the 96-well plate, 100 µL of the diluted cell suspension (1×10^4 cells) was added. After 24 hours, when a partial monolayer was formed, 100 µL of fresh medium with different compound concentrations (7.81, 15.625, 31.25, 62.5, 125, 250, 500 and 1000 µg mL^{-1}) were added to the cells. After 48 hours, the supernatant was washed out and 100 µL of MTT solution in medium (final concentration 0.5 mg mL^{-1}) were added to each well for 2 h. After the incubation time was complete, unreacted dye was removed by aspiration. The formazan crystals were dissolved in 100 µL per well DMSO and measured spectrophotometrically in a multi-well Synergy 2 plate reader (BioTek Instruments, USA) at a test wavelength of 492 nm and a reference wavelength of 690 nm. The results were calculated as an IC_{50} (inhibitory concentration 50) – the IC_{50} corresponds to the concentration of tested compound that inhibits cell viability/proliferation by 50%. Results are presented as mean of at least three independent experiments.

4.3.3 Colony formation assay. Colony formation assay is an *in vitro* cell survival assay base on the ability of single cell to grow a colony. The colony is defined to consist of at least 50 cells. The assay essentially tests every cell in the population for its ability to undergo unlimited division. Clonogenic assay is the

method of choice to determine cell reproductive death after treatment with ionizing radiation, but can also be used to determine effectiveness of other cytotoxic agents. Only a fraction of seeded cell retains the capacity to product colonies. The protocol was adapted from literature methods.[64] T98G and HaCaT cells were seeded in 6-well tissue culture plates at a density of 500 cells per well according to the morphology and growth patterns of each cell line, and were allowed adhere for 24 hours before treatment. The cells were treated with different compound concentrations (2 μM, 10 μM, 20 μM, 50 μM, 100 μM) for 7 days. Triplicate samples were used for each treatment. Medium containing the treatment was replaced with a compound-free medium after 24 h. Plates were rinsed in miliQ water and colonies were methanol-fixed and stained with 1% gentian violet and clones were counted under a light microscope.

4.3.4 In silico pharmacokinetic prediction. Calculations of pharmacokinetic profile descriptors of synthesized compounds were performed by various software solutions accessible online. The transformation of the stoichiometric formulas of the compounds into a SMILES code (Simplified Molecular Input Line Entry System) was carried out by ChemBioDraw Ultra version 12.0 program (Cambridge Software). The SMILES code was applied to calculate log *P* values (octanol/water partition coefficient), PSA (topological polar surface area) and aPSA (apolar surface area). The logP values were calculated by ALOGPS 2.1 software (http://www.vcclab.org/lab/alogps).[65] PSA and aPSA descriptors were calculated using the VEGA ZZ program (http://www.vegazz.net).[66] The pharmacokinetic profiles were also evaluated according to Lipinski's "rule of five"[67] by using Molinspiration application (http://www.molinspiration.com), which analyses molecular weight (MW), number of hydrogen-bond acceptors (HBA), and number of hydrogen-bond donors (HBD). The Caco-2 prediction model based on descriptors generated by preADMET (http://preadmet.bmdrc.org) was used to compute Caco-2 apparent permeability (t_{Papp}), for the tested compounds. In this model a number of hydrogen bond donors and three molecular surface area properties determine membrane permeability of compounds.

Conflicts of interest

There are no conflicts to declare.

Acknowledgements

This research was supported in part by PL-Grid Infrastructure (http://www.plgrid.pl/en).

References

1 Z.-Q. Zhu, L.-J. Xiao, D. Guo, X. Chen, J.-J. Ji, X. Zhu, Z.-B. Xi and Z.-G. Le, *J. Org. Chem.*, 2019, **84**, 435–442.
2 Z. Chen, P. Marce, R. Resende, P. M. Alzari, A. Carlos Frasch, J. M. H. van den Elsen, S. J. Crennell and A. G. Watts, *Eur. J. Med. Chem.*, 2018, **158**, 25–33.
3 V. M. S. Isca and A. C. Fernandes, *Green Chem.*, 2018, **20**, 3242–3245.
4 A. Mucha, P. Kafarski and Ł. Berlicki, *J. Med. Chem.*, 2011, **54**, 5955–5980.
5 X.-C. Huang, M. Wang, Y.-M. Pan, G.-Y. Yao, H.-S. Wang, X.-Y. Tian, J.-K. Qin and Y. Zhang, *Eur. J. Med. Chem.*, 2013, **69**, 508–520.
6 Q. Wang, L. Yang, H. Ding, X. Chen, H. Wang and X. Tang, *Bioorg. Chem.*, 2016, **69**, 132–139.
7 Z. Rezaei, H. Firouzabadi, N. Iranpoor, A. Ghaderi, M. R. Jafari, A. A. Jafari and H. R. Zare, *Eur. J. Med. Chem.*, 2009, **44**, 4266–4275.
8 I. Kraicheva, A. Bogomilova, I. Tsacheva, G. Momekov and K. Troev, *Eur. J. Med. Chem.*, 2009, **44**, 3363–3367.
9 Y.-C. Yu, W.-B. Kuang, R.-Z. Huang, Y.-L. Fang, Y. Zhang, Z.-F. Chen and X.-L. Ma, *MedChemComm*, 2017, **8**, 1158–1172.
10 B.-A. Song, Y.-L. Wu, S. Yang, D.-Y. Hu, X.-Q. He and L.-H. Jin, *Molecules*, 2003, **8**, 186–192.
11 F. R. Atherton, C. H. Hassall and R. W. Lambert, *J. Med. Chem.*, 1986, **29**, 29–40.
12 P. Kafarski and B. Lejczak, *Phosphorus, Sulfur Silicon Relat. Elem.*, 1991, **63**, 193–215.
13 F. Westheimer, *Science*, 1987, **235**, 1173–1178.
14 V. D. Romanenko and V. P. Kukhar, *Chem. Rev.*, 2006, **106**, 3868–3935.
15 S. A. Bernhard and L. E. Orgel, *Science*, 1959, **130**, 625–626.
16 K. V. Turcheniuk, V. P. Kukhar, G.-V. Röschenthaler, J. L. Aceña, V. A. Soloshonok and A. E. Sorochinsky, *RSC Adv.*, 2013, **3**, 6693–6716.
17 G. F. Makhaeva, A. Y. Aksinenko, V. B. Sokolov, I. I. Baskin, V. A. Palyulin, N. S. Zefirov, N. D. Hein, J. W. Kampf, S. J. Wijeyesakere and R. J. Richardson, *Chem.-Biol. Interact.*, 2010, **187**, 177–184.
18 E. P. Gillis, K. J. Eastman, M. D. Hill, D. J. Donnelly and N. A. Meanwell, *J. Med. Chem.*, 2015, **58**, 8315–8359.
19 B. E. Smart, *J. Fluorine Chem.*, 2001, **109**, 3–11.
20 S. L. Cobb and C. D. Murphy, *J. Fluorine Chem.*, 2009, **130**, 132–143.
21 L. D. Quin and G. S. Quin, *Comp. Biochem. Physiol., Part B: Biochem. Mol. Biol.*, 2001, **128**, 173–185.
22 M. Salwiczek, E. K. Nyakatura, U. I. M. Gerling, S. Ye and B. Koksch, *Chem. Soc. Rev.*, 2012, **41**, 2135–2171.
23 D. M. Ryan, S. B. Anderson, F. T. Senguen, R. E. Youngman and B. L. Nilsson, *Soft Matter*, 2010, **6**, 475–479.
24 H. Zheng, K. Comeforo and J. Gao, *J. Am. Chem. Soc.*, 2009, **131**, 18–19.
25 C. J. Pace, H. Zheng, R. Mylvaganam, D. Kim and J. Gao, *Angew. Chem., Int. Ed.*, 2012, **51**, 103–107.
26 G. Akçay and K. Kumar, *J. Fluorine Chem.*, 2009, **130**, 1178–1182.
27 C. J. Pace and J. Gao, *Acc. Chem. Res.*, 2013, **46**, 907–915.
28 S. E. Wheeler and K. N. Houk, *J. Chem. Theory Comput.*, 2009, **5**, 2301–2312.
29 T. Siodla, W. P. Oziminski, M. Hoffmann, H. Koroniak and T. M. Krygowski, *J. Org. Chem.*, 2014, **79**, 7321–7331.

30 F. Wang, L. Qin, P. Wong and J. Gao, *Org. Lett.*, 2011, **13**, 236–239.
31 L. Qin, C. Sheridan and J. Gao, *Org. Lett.*, 2012, **14**, 528–531.
32 A. M. Spokoyny, Y. Zou, J. J. Ling, H. Yu, Y.-S. Lin and B. L. Pentelute, *J. Am. Chem. Soc.*, 2013, **135**, 5946–5949.
33 J. Kwiczak-Yiğitbaşı, J.-L. Pirat, D. Virieux, J.-N. Volle, A. Janiak, M. Hoffmann and D. Pluskota-Karwatka, *Arabian J. Chem.*, 2018, DOI: 10.1016/j.arabjc.2018.05.002.
34 A. Pawlowska, J.-N. Volle, D. Virieux, J.-L. Pirat, A. Janiak, M. Nowicki, M. Hoffmann and D. Pluskota-Karwatka, *Tetrahedron*, 2018, **74**, 975–986.
35 S. A. Azizi and C. Miyamoto, *J. NeuroVirol.*, 1998, **4**, 204–216.
36 J. D. Lathia, S. C. Mack, E. E. Mulkearns-Hubert, C. L. L. Valentim and J. N. Rich, *Genes Dev.*, 2015, **29**, 1203–1217.
37 P. Anja, J. Anahid and K. Janko, *Semin. Cancer Biol.*, 2018, **53**, 168–177.
38 M. Sivaparvathi, R. Sawaya, S. W. Wang, A. Rayford, M. Yamamoto, L. A. Liotta, G. L. Nicolson and J. S. Rao, *Clin. Exp. Metastasis*, 1995, **13**, 49–56.
39 M. Sivaparvathi, M. Yamamoto, G. L. Nicolson, Z. L. Gokaslan, G. N. Fuller, L. A. Liotta, R. Sawaya and J. S. Rao, *Clin. Exp. Metastasis*, 1996, **14**, 27–34.
40 G. F. Makhaeva, S. V. Lushchekina, O. G. Serebryakova, A. Y. Aksinenko, T. V. Goreva, R. J. Richardson and I. V. Martynov, *Dokl. Biochem. Biophys.*, 2013, **451**, 203–206.
41 M. Sieńczyk and J. Oleksyszyn, *Curr. Med. Chem.*, 2009, **16**, 1673–1687.
42 J. Ajenjo, M. Greenhall, C. Zarantonello and P. Beier, *Beilstein J. Org. Chem.*, 2016, **12**, 192–197.
43 I. A. Khalfina and V. M. Vlasov, *Russ. J. Org. Chem.*, 2005, **41**, 978–983.
44 C. S. Gutsche, M. Ortwerth, S. Gräfe, K. J. Flanagan, M. O. Senge, H.-U. Reissig, N. Kulak and A. Wiehe, *Chem.–Eur. J.*, 2016, **22**, 13953–13964.
45 A. Bondi, *J. Phys. Chem.*, 1964, **68**, 441–451.
46 C. A. Lipinski, *Adv. Drug Delivery Rev.*, 2016, **101**, 34–41.
47 C. A. Lipinski, F. Lombardo, B. W. Dominy and P. J. Feeney, *Adv. Drug Delivery Rev.*, 1997, **23**, 3–25.
48 D. F. Veber, S. R. Johnson, H.-Y. Cheng, B. R. Smith, K. W. Ward and K. D. Kopple, *J. Med. Chem.*, 2002, **45**, 2615–2623.
49 M. Yazdanian, S. L. Glynn, J. L. Wright and A. Hawi, *Pharm. Res.*, 1998, **15**, 1490–1494.
50 X. Ma, C. Chen and J. Yang, *Acta Pharmacol. Sin.*, 2005, **26**, 500–512.
51 S. Lapointe, A. Perry and N. A. Butowski, *Lancet*, 2018, **392**, 432–446.
52 Q. T. Ostrom, L. Bauchet, F. G. Davis, I. Deltour, J. L. Fisher, C. E. Langer, M. Pekmezci, J. A. Schwartzbaum, M. C. Turner, K. M. Walsh, M. R. Wrensch and J. S. Barnholtz-Sloan, *Neuro-Oncology*, 2014, **16**, 896–913.
53 G. M. Sheldrick, *Acta Crystallogr., Sect. C: Struct. Chem.*, 2015, **71**, 3–8.
54 I. J. Bruno, J. C. Cole, P. R. Edgington, M. Kessler, C. F. Macrae, P. McCabe, J. Pearson and R. Taylor, *Acta Crystallogr., Sect. B: Struct. Sci.*, 2002, **58**, 389–397.
55 J.-D. Chai and M. Head-Gordon, *Phys. Chem. Chem. Phys.*, 2008, **10**, 6615–6620.
56 J. J. P. Stewart, *J. Comput. Chem.*, 1989, **10**, 209–220.
57 C. C. J. Roothaan, *Rev. Mod. Phys.*, 1951, **23**, 69–89.
58 J. B. Collins, P. von R. Schleyer, J. S. Binkley and J. A. Pople, *J. Chem. Phys.*, 1976, **64**, 5142–5151.
59 M. J. Frisch, G. W. Trucks, H. B. Schlegel, G. E. Scuseria, M. A. Robb, J. R. Cheeseman, G. Scalmani, V. Barone, G. A. Petersson, H. Nakatsuji, X. Li, M. Caricato, A. Marenich, J. Bloino, B. G. Janesko, R. Gomperts, B. Mennucci, H. P. Hratchian, J. V. Ortiz, A. F. Izmaylov, J. L. Sonnenberg, D. Williams-Young, F. Ding, F. Lipparini, F. Egidi, J. Goings, B. Peng, A. Petrone, T. Henderson, D. Ranasinghe, V. G. Zakrzewski, J. Gao, N. Rega, G. Zheng, W. Liang, M. Hada, M. Ehara, K. Toyota, R. Fukuda, J. Hasegawa, M. Ishida, T. Nakajima, Y. Honda, O. Kitao, H. Nakai, T. Vreven, K. Throssell, J. A. Montgomery Jr, J. E. Peralta, F. Ogliaro, M. Bearpark, J. J. Heyd, E. Brothers, K. N. Kudin, V. N. Staroverov, T. Keith, R. Kobayashi, J. Normand, K. Raghavachari, A. Rendell, J. C. Burant, S. S. Iyengar, J. Tomasi, M. Cossi, J. M. Millam, M. Klene, C. Adamo, R. Cammi, J. W. Ochterski, R. L. Martin, K. Morokuma, O. Farkas, J. B. Foresman, and D. J. Fox, *Gaussian 09, Revision A.02*, Gaussian, Inc., Wallingford CT, 2016.
60 P. Atkins and J. de Paula, *Physical Chemistry*, W. H. Freeman, New York, 9th edn, 2009.
61 H. Shanan-Atidi and K. H. Bar-Eli, *J. Phys. Chem.*, 1970, **74**, 961–963.
62 K. Salus, M. Hoffmann, T. Siodła, B. Wyrzykiewicz and D. Pluskota-Karwatka, *New J. Chem.*, 2017, **41**, 2409–2424.
63 C. P. R. Xavier, C. F. Lima, M. Rohde and C. Pereira-Wilson, *Cancer Chemother. Pharmacol.*, 2011, **68**, 1449–1457.
64 L. C. Crowley, M. E. Christensen and N. J. Waterhouse, *Cold Spring Harb. Protoc.*, 2016, DOI: 10.1101/pdb.prot087171.
65 I. V. Tetko, J. Gasteiger, R. Todeschini, A. Mauri, D. Livingstone, P. Ertl, V. A. Palyulin, E. V. Radchenko, N. S. Zefirov, A. S. Makarenko, V. Yu. Tanchuk and V. V. Prokopenko, *J. Comput.-Aided Mol. Des.*, 2005, **19**, 453–463.
66 A. Pedretti, L. Villa and G. Vistoli, *J. Mol. Graphics Modell.*, 2002, **21**, 47–49.
67 C. A. Lipinski, F. Lombardo, B. W. Dominy and P. J. Feeney, *Adv. Drug Delivery Rev.*, 2001, **46**, 3–26.